UNIVERSITÀ DEGLI STUDI DI MILANO
FACOLTÀ DI SCIENZE MATEMATICHE FISICHE E NATURALI
LAUREA SPECIALISTICA IN FISICA

Statistical properties of the random 2-dimensional euclidean Grid-Poisson Marriage problem

Relatore: Prof. Sergio Caracciolo
Correlatore: Dott. Andrea Sportiello

Laureando: Elia Zarinelli
Matr. n. 720131

Codice PACS: 02.50.-r

ANNO ACCADEMICO 2007-2008

Contents

Chapter 1

The Grid-Poisson Marriage

In this chapter we will introduce basic definitions of graph theory and combinatorial optimization; we will present the Grid-Poisson Marriage, the model of statistical mechanics that we will study in this work, and his connections with the Assignment problem, a classical problem of combinatorial optimization.

1.1 Introduction

Graph theory, combinatorial optimization and statistical physics are disciplines with a huge overlap between each other.

One of the main aims of statistical physics is to describe phase transitions and critical phenomena; the natural framework for describe the physical world is the continuous space, with all the benefits coming from the symmetries that a continuous model may enjoy; statistical physics renounces using this framework to adopt the discrete space, which is described with the mathematical language of graph theory. To appreciate the goodness of this choice, we can think to the amount of results obtained since when, in late 1920, Lenz introduced the discrete model which would have become famous with the name of his student Ising. In the other hand, also graph theory obtained benefits from statistical physics; an old example of this is the work of Kasteleyn (a physicist) who introduced a method for counting perfect matchings over planar graphs (a discrete mathematics problem). At the same time graph theory is the natural framework to describe problems of combinatorial optimization.

One of the most exciting challanges of modern statistical physics is the description of disordered systems, with the prototipe example of spin

glasses; in the last thirty years a set of sophisticated mathematical methods, like Replica and Cavity Method, have been introduced to understand these systems; such new developments have found a natural field of application in combinatorial optimization, and it is not surprising that one of first accounts of such methods [1] devoted one section to applications in optimization problems. Also common methods of combinatorial optimization hasve been used for a better comprehension of disordered systems.

We have then seen that this situation of overlap has led to a transgression of boundaries so that progress in one discipline can benefit the others.

1.2 About graphs

A *directed graph* $G = (V, E)$ consists in a set of *vertices* V and a set of *arcs* $E \subseteq V^2$; every arc (u, v) joins two – possibly identical – vertices u and v. We say that an arc (u, v) is incident from u and incident to v.

An *undirected graph*, or *graph*, is a directed graph with symmetric incidence relation: if (u, v) is in the arc-set of G, then also (v, u). Hence we call such a pair of arcs an *edge* incident to u and v. The vertex set of a graph G is referred to as $V(G)$ and the edge set $E(G)$. A *weighted graph* is a graph together with a weight-function on his edges: $w : E(G) \to \mathbb{R}$.

Two vertices joined by an edge are said *adjacent*. The *neighbourhood* $\mathcal{N}_G(v)$ of a vertex is the set of vertices adjacent to it. The *degree* $\deg_G(v)$ of a vertex is the number of edges incident to it. If all the vertices of a graph G have same degree k, G is said *k-regular*. The *complete* graph $\mathcal{K}_n$ is a graph with n vertices and each pair of vertices is joined by an edge; thus the complete graph is $(n-1)$-regular.

A graph is said *bipartite* if it is possible to separate its vertex set in two classes, so that its edges join only vertices belonging to different classes. A *complete bipartite* graph $\mathcal{K}_{m,n}$ is a bipartite graph with m vertices in a class and n vertices in the other class, where each pair of vertices belonging to different classes is joined by an edge.

We call $S = (V', E')$ a *subgraph* of a graph $G = (V, E)$ if $V' \subseteq V$, $E' \subseteq E$ and V' contains all the vertices adjacent to E'. If $V(S) = V(G)$ we say that S is *spanning* in G.

A *matching* of a graph G is a subset $M \subseteq E(G)$ such that $\forall v \in V(G)$ at most one edge in M is incident in v. The size of a matching $|M|$ is the

Figure 1.1: Left: the complete bipartite graph $\mathcal{K}_{3,4}$; right: a maximum matching of the complete bipartite graph $\mathcal{K}_{3,4}$ (dark lines).

number of edges in M; a *maximum matching* is a matching M such that every other matching M' satisfies $|M'| \leq |M|$. If the graph G is a weighted graph, the weight of a matching is the sum of the weights of edges in M.

A *walk* w in a graph $G = (V, E)$ connecting w_0 with w_k is a sequence $(w_0, e_1, w_1, e_2, w_3, \ldots, e_k, w_k)$ such that all $w_i \in V$, all $e_i \in E$ and $(w_{i-1}, w_i) = e_i$ for $1 \leq i \leq k$. A *loop* is a walk connecting the starting point w_0 with itself. A *path* in G is a walk in which $w_0, \ldots, w_k$ are distinct vertices of G and $e_1, \ldots, e_k$ are distinct edges of G. A *cycle* in G is a walk in which:

a) $w_0, \ldots, w_{k-1}$ are distinct vertices of G, and $w_k = w_0$,

b) $e_1 \ldots, e_k$ are distinct edges of G,

c) $k \geq 2$.

A graph G is said to be *connected* if every pair of vertices in G can be connected by a walk. The *connectd components* of G are the maximal connected subgraphs of G. We denote by $k(G)$ the number of connected components of G.

A *forest* is a graph that contains no cycles. A *tree* is a connected forest (thus, the connected components of a forest are trees).

For every graph $G = (V, E)$ is valid the *Euler formula*, which relates the number of vertices $|V(G)|$, the number of edges $|E(G)|$, the number of connected components $k(G)$ and the number of independent loops $L(G)$:

$$|V(G)| + L(G) = |E(G)| + k(G). \tag{1.1}$$

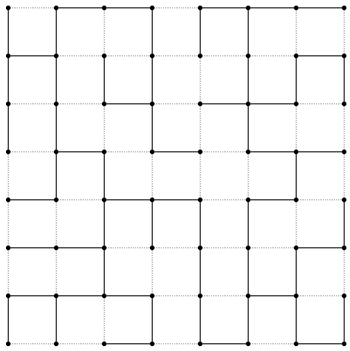

Figure 1.2: A spanning tree subgraph for the 8×8 square graph.

1.3 A short introduction to combinatorial optimization

Combinatorial optimization is a branch of computer science that tries to solve problems that descend mainly from practice and every-day life. Even in the very primitive human societies, finding short paths and searching (for instance for food) were essential problems to solve. An example is the following:

> *Given a number of cities and the cost of traveling from a city to any other city, what is the least-cost round-trip route that visits each city exactly once and then returns to the starting city?*

This problem (known as Travelling Salesman Problem, TSP) crops up when you plan sightseeing or when a doctor or a mailman plans his tour. Similarly, assigning jobs to men, trasporting goods and making connections are elementary problems, not just fot mathematicians.

From a mathematical point of view, basic ingredients of a combinatorial optimization problem are: an **instance** (in the TSP, the set of cities and the set of costs of traveling), a finite space of **feasible solutions** (in the TSP, all the possible round-trips with requested properties) and a **cost function** over the space of feasible solutions (in the TSP, the total cost of every round-trip). The optimization problem is solved when, given an instance, a feasible solution which minimizes the cost function is found.

Optimization problems can often be given in mathematical terms with the use of graph theory. Here we give a list of optimization problems

defined on a connected weighted graph $G = (V, E)$.

- *Min-Cut Problem*: it is desired to find the cut of minimum cost for the graph G. A subset of edges is called a cut if it is such that when these edges are removed from G, the graph becomes disconnected.
- *Minimum Spanning Tree Problem*: it is desired to find the minimum cost spanning tree subset of G.
- *Chinese Postman Problem*: it is desired to find the loop of minimum lenght that passes through every edge at least once.
- *Assignment Problem*: given a bipartite weighted graph G this problem consists in finding the optimal maximum matching of the graph G; the optimal maximum matching it's the maximum matching with minimal weight.

We are interested to find the solution of problems via algorithms. An algorithm is, loosely speaking, a procedure for solving a problem. More precisely it is a set of instructions understandable by an appropriate automatic machine, such that, given some input data, in a finite number of steps, leads to some output.

Since the space of feasible solutions is finite, it is always possible to find an algorithm that "solves" the problem; we can think to the naïve algorithm that assigns to every feasible solution his cost and pick up the best one.

But this kind of solution is not satisfactory. We can understand why if we think to the TSP; if the number of cities is n, we easily find that the number of possible tours is $(n-1)!/2$; now suppose that the naïve algorithm runs 1 second, on a given machine, to solve the problem if the number of cities is $n = 20$. Then to solve the problem with $n = 40$ cities it will need $39!/19! \gg 20^{20}$ seconds. In fact this algorithm finds the solution, but we will not live enought to see it.

So we change our definition of "solving" the problem; we say that an algorithm "solves" a problem if the required number of elementary steps needed by the algorithm to find the solution is bounded by a polynomial in the size of the problem. The size of the problem can be assumed to be the number of bits needed to encode it.

All the problems listed above have been solved in this sense, but there are problems that have not been; here we liste some examples.

- *Max-Cut Problem*: it is desired to find the cut with maximal cost.

- *Steiner Network Problem* : for a given set of points (for example in the plane) the Steiner network is the shortest set of edges which connects all of them.

- *Traveling Salesman Problem*

- *K-Satisfiability Problem*: given a set of N boolean variables and M clauses, each of them involving exactly K literals, the problem consists in finding (if it exists) a configuration of the variables such that every clause is satisfied.

This is a very short and naïve introduction to combinatorial optimization; if the reader is interested in a complete and rigorous one can see for example [4].

1.4 The model

After this short introduction to combinatorial optimization, we present the model of statistical mechanics that we will study in this work: the Grid-Poisson Marriage (GPM); we will see that this is strictly related to the assignment problem described before. There is some study of this model in litterature [2] or related models [3] .

Consider the square $[0, L] \times [0, L] \subset \mathbb{R}^2$ in the plane, with L integer; in the square is defined the euclidean distance $d(a, b) = ((x_a - x_b)^2 + (y_a - y_b)^2)^{1/2}$. We will call **grid points** the discrete subset of points of the square, defined by:

$$\mathcal{G} = \{(i - 0.5, j - 0.5) \in [0, L] \times [0, L] : i \in (1, 2, \ldots, L), j \in (1, 2, \ldots, L)\}.$$

We define N as the number of grid points: $N := |\mathcal{G}| = L^2$.

We define an instance of **Poisson points** as the discrete subset of the square:

$$\mathcal{P} = \{(x_i, y_i) \in [0, L] \times [0, L] : i \in (1, 2, \ldots, M)\},$$

where x_i and y_i are i.i.d. random variables with uniform distribution in $[0, L]$; the number of Poisson points is $M := |\mathcal{P}| \geq N$. A mathematician would say that an instance of Poisson points is the support of a point process. A point process is the rigorous formulation of "take random discrete subsets of points in a given set" in terms of random measures. If the reader

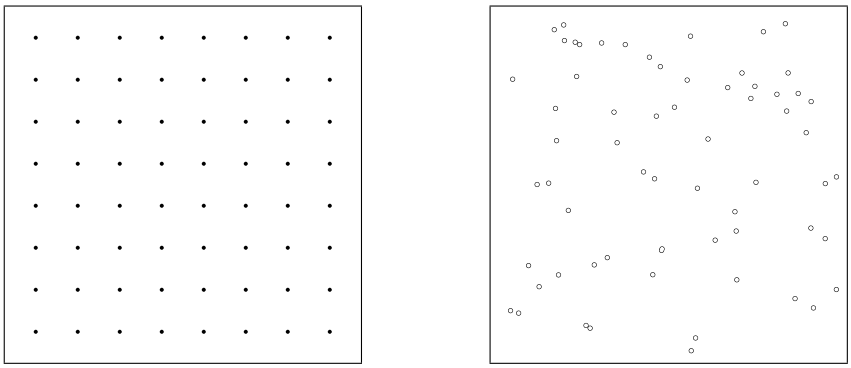

Figure 1.3: Left: grid points in a square of side $L = 8$. Right: an instance of $N = 64$ Poisson points.

is interested to a complete exposition of the argument we refer to [5].

Given an instance of Poisson points, we define a **marriage** between grid and Poisson points as a function $\pi : \mathcal{G} \to \mathcal{P}$ that marries a grid point to a Poisson point, such that every Poisson point is married to no more than a single grid point.

We define the energy of a marriage π as the sum of the distances between married points:

$$H_{\mathcal{P}}(\pi) = \sum_{i}^{N} d(i, \pi(i)).$$

We will call π_{opt} the marriage with minimum energy; we define the **energy** of an instance of Poisson points as the energy of π_{opt}:

$$H(\mathcal{P}) := H_{\mathcal{P}}(\pi_{opt}) = \min_{\pi} H_{\mathcal{P}}(\pi).$$

Then, to find the energy of an instance of Poisson points, we have to solve a problem of combinatorial optimization, where the space of feasible solutions is the set of all the possible marriages – if $|\mathcal{G}| = |\mathcal{P}| = N$ the number of possible marriages in $N!$ – and the cost function to minimize is the energy $H_{\mathcal{P}}(\pi)$.

We give a graphical representation of this problem; consider a complete bipartite weighted graph $\mathcal{K}_{N,M}$, with $V(\mathcal{K}_{N,M}) = \mathcal{G} \cup \mathcal{P}$ and weight function $w((i,j)) = d(i,j)$. The problem of finding the energy of an instance of Poisson points is equivalent to the problem of finding the optimal maximum matching of the graph $\mathcal{K}_{N,M}$.

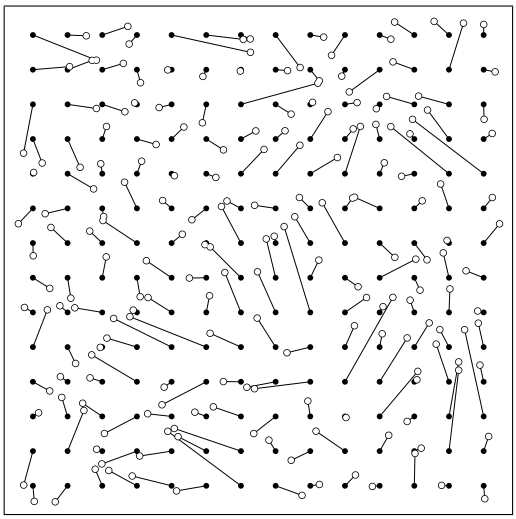

Figure 1.4: The optimal marriage (π_{opt}) of 196 grid points and 196 Poisson points.

This is the assignment problem, introduced before, that we will describe in the next section.

1.5 The assignment problem

There are many "pictorial" representations of the assignment problem[1].

For example one can consider to have N jobs to do and M machines, $M \geq N$, that can do them; every machine can do only a job and it is given a set of costs $\epsilon = \{\epsilon_{ij}\}$ for executing the i-th job on the j-th machine. The goal is to assign every job to a different machine, minimizing the total cost

[1] The assignment problem is one of the first studied combinatorial optimization problems. It was investigated by G. Monge in 1784 [6], camouflaged as a continuous problem, and often called a transportation problem. Monge described the problem as follows:

> Lorsqu'on doit transporter des terres d'un lieu dans un autre, on a coutime de dnner le nom de Déblai au volume des terres que l'on doit transporter, & le nom de Remblai a l'espace qu'elles doivent occuper après le transport.
>
> Le prix du transport d'une molécule étant, toutes choses d'ailleurs égales, proportionnel a son poids & a l'espace qu'on lui fait parcourir, & par conséquent le prix du transport total devant être proportionnel a la somme des produits des molécules multipliées chacune par l'espace parcouru, il s'ensuit que le déblai & le remblai étant donnés de figure & de position, il n'est pas indifférent que telle molécule du déblai soit transportée dans tel ou tel autre endroit du remblai, mais qu'il y a une certaine distribution a faire des molécules du premier dans le second, d'après laquelle la somme de ces produits sera la moindre possible, & le prix du transport total sera un *minimum*.

More information can be found in [7].

for executing the jobs. We will call a valid *assignment* a map that assigns to every job a different machine.

Then for this combinatorial optimization problem an instance is a set of costs ϵ, the set of feasible solutions is the set of valid assignments and the cost function on the set of feasible solutions is the function that gives to every valid assignment the sum of the costs of the jobs prescribed by this assignment.

Suppose that the number of machines is equal to the number of jobs: $M = N$. We have the following representations of the problem.

- A valid assignment can be associated to a permutation π of the symmetric group $\mathcal{S}_N$; the cost function can be written as:

$$H_\epsilon(\pi) = \sum_{i=1}^{N} \epsilon_{i\pi(i)} \, .$$

- Another useful representation is more "algebraic". We can encode a permutation π through a $N \times N$ matrix n_{ij} valued on $\{0, 1\}$, such that $n_{i\pi(i)} = 1$ and $n_{ij} = 0$ for $j \neq \pi(i)$. In this reformulation the set of feasible solutions is composed by the set of matrices $N \times N$ valued on $\{0, 1\}$ with the costraints:

$$\sum_{i=1}^{N} n_{ij} = 1 \quad \forall \, j \in \{1, \ldots, N\} \, , \qquad \sum_{j=1}^{N} n_{ij} = 1 \quad \forall \, i \in \{1, \ldots, N\} \, ;$$

  and the cost function is:

$$H_\epsilon(n) = \sum_{i,j} \epsilon_{ij} n_{ij} \, .$$

- We then also give the graphical representation. Consider a complete bipartite weighted graph $\mathcal{K}_{N,N}$ with $V(\mathcal{K}_{N,N}) = V_r \cup V_c$, where V_r is the set of jobs and V_c is the set of machines, and a weight function $w((i, j)) = \epsilon_{ij}$. Then the set of feasible solutions is composed by the set of maximum matchings of the graph $\mathcal{K}_{N,N}$, and the cost function is the weight of the matchings.

If the instance ϵ has a single assignment π realizing the minimum, we say that it is *non-degenerate*, and conversely, if there are two or more assignments with optimal cost, we say that the instance is degenerate.

Looking at the graphical representation of the assignment problem and of the GPM, we see that the GPM is a particular case of the assignment problem; let us underline this difference. If we think to the pictorial representation of the assignment problem in terms of jobs and machines, we can suppose that every cost ϵ_{ij} is independent from other costs; for example we can choose them random in $[0, 1]$ and then solve the problem. For the GPM this is no more true: the costs ϵ_{ij} are not independent because subjected to geometrical constraints.

Now we explain how the Hungarian algorithm finds the solution of this problem.

1.5.1 Gauge invariance

Given two real-valued vectors with N components λ and μ, we introduce a $2N$-parameter family of transformations $\Phi = \Phi_{\lambda,\mu}$ that assigns to every set of costs ϵ a new set of costs $\epsilon' = \Phi_{\lambda,\mu}(\epsilon)$, defined as:

$$\epsilon'_{ij} = \epsilon_{ij} - \lambda_i - \mu_j \, .$$

This family of transformations, that we will call *gauge transformations*, has the property of leave the problem unchanged. In fact, for every assignment π, it is easy to check that:

$$H_\epsilon(\pi) = H_{\epsilon'}(\pi) + h_0 \;\; ; \qquad h_0 = \sum_i \lambda_i + \sum_j \mu_j \, .$$

This means that every feasible solution π has the same energy in the old and in the new problem, up to a shift of h_0, independent from π and thus irrelevant at the aim of finding the optimal assignment.

We will call a gauge transformed matrix ϵ' accessible from a given ϵ simply *gauge*. The space of gauges ϵ' is in bijection with the pairs of vectors (λ, μ) and inherits from this the topology and the metric of R^{2N}, so it makes sense to say that a subset of gauges is *connected*, or *compact*, or *convex*.

We will call a gauge ϵ' *proper* if every element ϵ'_{ij} is non-negative. We assign to every proper gauge ϵ' the spanning subgraph $Z_{\epsilon'}$ of the complete bipartite graph $\mathcal{K}_{N,N}$ whose edges (i, j) are the ones such that $\epsilon'_{ij} = 0$.

Starting from a proper gauge ϵ and performing a gauge transformation to another proper gauge ϵ', h_0 is a trivial lower bound to the cost of the

optimal assignment for ϵ. In fact:

$$0 \leq H_\epsilon(\pi_{opt}) = \min_\pi H_\epsilon(\pi) = \min_\pi H_{\epsilon'}(\pi) + h_0 \ ;$$

since $\min_\pi H_{\epsilon'}(\pi) \geq 0$, then $H_\epsilon(\pi_{opt}) \geq h_0$. Not only, if one could find an assignment π such that $H_{\epsilon'}(\pi) = 0$, which means $\epsilon'_{i\pi(i)} = 0$ for all i, this certificates that π is an optimal assignment for ϵ, with cost exactly h_0. From a graphical point of view:

> *given a gauge transformation $\Phi_{\lambda,\mu}$ from a proper gauge ϵ to another proper gauge ϵ', if the graph $Z_{\epsilon'}$ contains a matching of size N, then the assignment associated to the matching is the optimal assignment for the instance ϵ, and the cost of the optimal assignment is the h_0 given by the gauge transformation.*

We call a proper gauge ϵ *Hungarian* if the corresponding Z_ϵ contains a matching of size N.

This is the basic idea of the Hungarian algorithm, that we will describe in the next section: starting from a proper gauge, perform a series of gauge transformations, until we get a Hungarian gauge.

We call a *gauge proper and non-trivial* if every row and every column of ϵ' contains at least one zero (this means that no vertex in $Z_{\epsilon'}$ is isolated). Clearly, this is a necessary but not sufficient condition for being Hungarian.

A proper non-trivial gauge is easily found for every instance ϵ, e.g. by composing first the gauge with $\mu_j = 0$ and $\lambda_i = \min_j(\epsilon_{ij})$, and then applying to the resulting gauge ϵ' the analogous transformation with $\lambda_i = 0$ and $\mu_j = \min_i(\epsilon'_{ij})$. We call $\Phi^{trivial}$ the map above, which acts as a projector from the space of proper gauges to the subspace of proper non-trivial gauges, and increases h_0 by the amount $\sum_j \min_j(\epsilon_{ij}) + \sum_i \min_i(\epsilon'_{ij}) \geq 0$.

1.6 The Hungarian Algorithm

A classical algorithm for the assignment problem which finds an optimal matching in polynomial time (worst-case) is due to H. Kuhn [8], who called it "Hungarian algorithm" as a tribute to the mathematicians authors of the two main lemmas on which is based, Kőnig and Egerváry.

Consider the complete bipartite graph $\mathcal{K}_{N,N}$, with $V(\mathcal{K}_{N,N}) = V_c \cup V_r$, and a spanning subgraph Z of $\mathcal{K}_{N,N}$. For $X \subseteq V_r$, let $\mathcal{V}(X)$ denote the

subset of verte of V_c connected to some vertex in X with an edge in Z. The difference of the two cardinalities, $d(X) := |X| - |\mathcal{V}(X)|$, is called the deficit number of X. Consider a matching M in Z, let $\mathcal{N}(M)$ the number of unmatched elements in V_c by the matching M. Then we have the following theorem.

Theorem 1 (Kőnig 1916)**.** *In a bipartite graph $Z = (V_c \cup V_r, E)$ the minimum number of unmatched elements in V_r, $\mathcal{N}(M)$, over all the possible matchings is equal to the maximum over all the subsets X of the deficit number $d(X)$:*

$$\min_M \mathcal{N}(M) = \max_X d(X) \, .$$

As a corollary, the graph Z has a matching of size N if and only if $|\mathcal{V}(X)| \geq |X|$ for all $X \subseteq V_r$.

It is possible to give a constructive proof of the theorem [4] and then apply some idea of the proof to obtain a maximum matching algorithm.

Egerváry theorem, instead, uses Kőnig's results in weighted bigraphs (over which is defined the assignment problem, and his converse the maximum weighted matching problem). We present it with the language used in section of gauge invariance.

Theorem 2 (Egerváry 1931)**.** *The cost of the optimal assignment is equal to the maximum value of $h_0 = \sum_i \lambda_i + \sum_j \mu_j$ a proper gauge can have. So, a proper gauge that realizes the maximum h_0 in the whole set of proper gauges has the property that its graph of zeroes Z admits a matching. Such a gauge always exists.*

The first part of the theorem is proven, e.g. in [9], constructively through Kőnig theorem. We will show the existence of solutions.

We already know that the set of non-trivial proper gauges is non-empty, since, for every proper gauge ϵ, $\Phi^{trivial}$ always exists, so let $\epsilon' = \Phi^{trivial}(\epsilon)$ with $h_0(\epsilon') \geq 0$. Then, given any non-trivial proper gauge ϵ' such that $Z_{\epsilon'}$ does not admit a matching, by Kőnig theorem there exists $X \subseteq V_r$ with positive deficit $d(X)$. We can construct a further gauge transformation $\Phi_{\lambda,\mu}$ with parameters:

$$\lambda_i = \begin{cases} \delta & i \in X \\ 0 & i \notin X \end{cases} \quad \mu_j = \begin{cases} -\delta & j \in \mathcal{V}(X) \\ 0 & j \notin \mathcal{V}(X) \end{cases} \quad \delta = \min_{\substack{i \in X \\ j \in V_c \setminus \mathcal{V}(X)}} (\epsilon'_{ij})$$

which applied to ϵ' gives a new non-trivial proper gauge ϵ'' with $h_0(\epsilon'') = \delta \cdot d(X)$; since $\delta > 0$, $h_0(\epsilon'')$ is positive.

This proves that non-trivial proper gauges which are not Hungarian cannot be local maxima of h_0, and from compactness of the set of non-trivial proper gauges (with a opportune quotient) and the fact that h_0 is a continuous function of parameters (λ, μ) we conclude that the set of Hungarian gauges is non-empty.

This mechanism sheds some light on the structure of the problem. "Hard" problems in computational complexity are expected to show the emergence of a pseudo-glassy structure in the phase space, such that a blind local search gets trapped in local minima. Conversely, if all the local minima are also global, and all other points have finite gradient, one could hope to reach a minimum by local search. Assignment problem is not hard, as it is polynomial, but it is not either a trivial problem, and the theorem above shows that, under a well chosen parametrization, a steepest descending algorithm finds the global minimum.

Egerváry theorem seems to be the solution of the problem: just project ϵ through $\Phi^{trivial}$, device some method to find a positive-deficit set X in polynomial time, and apply a sequence of gauge transformations up to saturate the upper bound.

Actually, this is not enough. Indeed, the compactness argument only proves an existence statement and that a sequence of gauges would induce a monotonically increasing sequence of h_0, but, as we do not have a positive lower bound on the gain $\delta \cdot d(X)$ attained at each step, the naïve application of the theorem would not provide a polynomial algorithm.

As showed by Khun, the algorithm can be proven to be strongly polynomial if in each gauge transformation the set X in Egerváry theorem is chosen with the appropriate prescription, namely to choose the X which has the smaller size, among the ones with maximum deficit.

The implementation of the Hungarian algorithm, that we have used to perform simulations in our work, done by Knuth [10], has a worst-case complexity upper bound of $\mathcal{O}(n^3)$. We would also stress the fact that in the GPM the size of the model is $n = L^2$, then, if we consider the side of the square, we would have a worst-case complexity upper bound of $\mathcal{O}(L^6)$.

Chapter 2

Super-extensivity of the Energy

In the previous chapter we have given a short introduction to combinatorial optimization and we have seen how the Hungarian algorithm finds the solution of the assignment problem. We have also seen that, given an instance of Poisson points for the GPM, if we construct the distance matrix ϵ, with entrance ϵ_{ij} equal to the distance between the i-th grid point and the j-th Poisson point, we can use the Hungarian algorithm to find the optimal matching and his energy.

We also remember that:

$$H(\mathcal{P}) := H_{\mathcal{P}}(\pi_{opt}) = \min_{\pi} H_{\mathcal{P}}(\pi)$$

and that Poisson points are taken with uniform distribution in the square. Then we can define $\langle H(\mathcal{P})\rangle_{\mathcal{P}}$ as the average of $H(\mathcal{P})$ over this probability distribution.

In this chapter we will study $\langle H(\mathcal{P})\rangle_{\mathcal{P}}$ as a function of the size N of the system and of the number M of Poisson points; if we define a density $\rho := M/N$, we will discover a particular behaviour for $\rho = 1$.

At this point, the reader familiar with the argument may remember the well-known Parisi conjecture for the random assignment problem. Parisi and Mèzard in [11] used the replica theory to study the assignment problem in which the matrix elements ϵ_{ij} were random variables taken with uniform distribution in $[0, 1]$. This allowed to calculate the mean value of the energy $\langle H(\epsilon)\rangle_{\epsilon}$ at a given size N. In 1998 Parisi [12] conjectured that, in the case where the probability distribution of each matrix element ϵ_{ij} were $p(\epsilon_{ij}) = \exp(-\epsilon_{ij})$, the mean value of the energy at a given size N was: $\langle H(\epsilon)\rangle_{\epsilon}(N) = \sum_{k=1}^{N} \frac{1}{k^2}$, and in particular $\lim_{N\to\infty}\langle H(\epsilon)\rangle_{\epsilon}(N) = \pi^2/6$.

This conjecture was proved by Aldous in 2001 [13] and by Nair et al. in 2005 [14].

As underlined before, the GPM differs from the random assignment problem for the geometrical constraints to which are subjected the costs ϵ_{ij}. These constraints make also very difficult perform analytically the statistical average. To overcome this difficulty we will introduce a heuristic to obtain an upper-bound for $\langle H(\mathcal{P})\rangle_{\mathcal{P}}$, and then we will perform numerical simulations. We see that in random assignment problem, by Parisi conjecture, for $N \to \infty$ the energy becomes a constant; for the geometrical properies of GPM, it's easy to show that in this case the energy is at least extensive in the size N of the square.

Let us explain what we mean with heuristic. We have said that in combinatorial optimization the goal is to find the feasible solution that minimizes the cost function; sometimes this can need hard efforts. A heuristic algorithm (or simply a heuristic) is an algorithm that gives up finding the optimal solution, but can be faster or easier to understand compared with the optimal one. In the following we present two heuristic algorithms for the GPM: the *Stable marriage algorithm* and the *Box algorithm*.

2.1 The Stable marriage algorithm

Consider two discrete sets of points $U, V \subseteq \mathbb{R}^d$ and a marriage of U in V. Following Gale and Shapley [15], we will say that the marriage π is stable if do not exist two points $x \in U$ and $y \in V$ satisfying:

$$|x - y| < \min\{|x - \pi(x)|, |y - \pi(y)|\}, \tag{2.1}$$

where $|x - \pi(x)| := \infty$ if x is unmarried. A pair x, y satisfying (2.1) is called unstable (the motivation for this definition is that each point prefers to be married with closer points, so an unstable pair x, y prefer to divorce their current partners and marry each other).

The following algorithm, a "greedy" algorithm that tries to optimize locally, finds the stable marriage of two discrete sets of points $U, V \subseteq \mathbb{R}^d$. We will say that $x \in U$ and $y \in V$ are mutually closest if y is the closest point to x in V and x is the closest point to y in U. Given a point configuration, marry all mutually closest pairs to each other, then remove these points and marry all mutually closest pairs in the remaining set of points. Repeat indefinitely. Since at every round the number of mutually closest

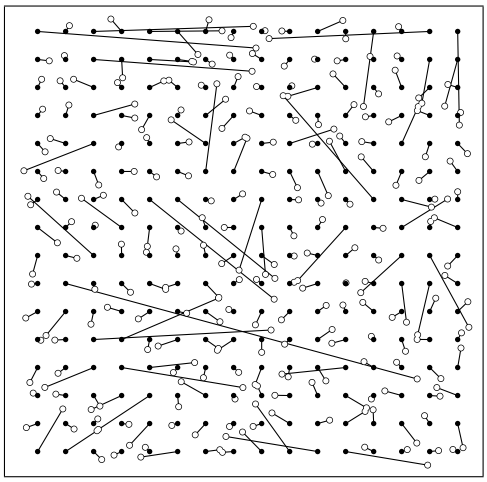

Figure 2.1: An example of π_{st} on a square of size $L = 16$.

pairs is greater or equal to one, the algorithm stops in a finite number of rounds.

There is also a pictorial representation of the algorithm. Grow a ball centered at each point in U (U-balls) and at each point in V (V-balls) simultaneously, so that at time t all the balls have radius t. Whenever a U-ball and a V-ball touch, match their centers to each other, and remove the two balls. This kind of pictorial representation can also be seen in [16].

If we consider as discrete subsets of $\mathbb{R}^2$ the sets $\mathcal{G}$ and $\mathcal{P}$, we can apply the Stable marriage algorithm to the GPM; we will call π_{st} the marriage found by the Stable marriage algorithm (see an example in fig. 2.1). Obviously this inequality holds:

$$H_{\mathcal{P}}(\pi_{opt}) \leq H_{\mathcal{P}}(\pi_{st}).$$

This means that the Stable marriage algorithm is a heuristic for the GPM. We have implemented the Stable marriage algorithm, that is polynomial, and with a suitable implementation has the bound in $\mathcal{O}(n^2)$.

2.2 The Box algorithm

The box algorithm is an algorithm of the kind "divide and conquer".

Consider the GPM with $N = 2^{\bar{k}}$ grid points – with $\bar{k}$ even such that $L = 2^{\bar{k}/2}$ – and an instance of M Poisson points.

For any $k = 0, \dots, \bar{k}$, we consider the natural subdivision of the square of side L in: squares of area 2^k if k is even, rectangles of area 2^k and ratio $1/2$ if k is odd; we can see an example of these subdivisions in figure 2.2. Then there are pairings of k-boxes that give $(k+1)$-boxes.

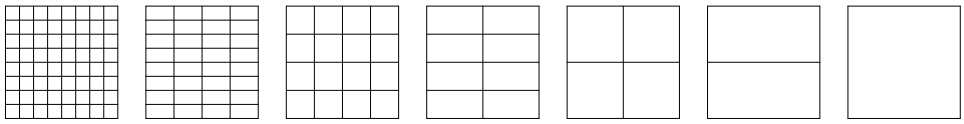

Figure 2.2: A square of side $L = 8$ divided in 0-boxes, 1-boxes and so on.

We introduce a parameter that will be useful in the following: if h_c is the number of Poisson points in a k-box c, we define q_c as the difference of the number of Poisson points and of grid points present in the k-box c: $q_c := h_c - 2^k$; then $q_c \in \{-2^k, \dots, N - 2^k\}$.

The steps of the algorithm are the following:

Preparatory step of the algorithm: divide the square in $2^{\bar{k}}$ 0-boxes; in every box, if possible, marry the grid point to a Poisson point (chosen randomly) in the same box and remove the married pair.

k-th step of the algorithm: divide the square in $N/2^{k+1}$ $(k+1)$-boxes; within each $(k+1)$-box, marry as many grid-Poisson pairs as possible (choose randomly a pair and remove it).

After the preparatory step, the algorithm starts with the 0-step and stops at the $(\bar{k}-1)$-step. At the end every grid point will be married to a Poisson point and we call π_{box} the obtained marriage. The energy of π_{box} is the sum of the energies resulting from the preparatory step, E_{prep}, and from every k-step, $E(k)$:

$$H_{\mathcal{P}}(\pi_{box}) = E_{prep} + \sum_{k=0}^{\bar{k}-1} E(k). \tag{2.2}$$

Since the choices perfomed by the Box algorithm are sub optimal to the one performed by Stable marriage algorithm, the following inequality holds:

$$H_{\mathcal{P}}(\pi_{opt}) \leq H_{\mathcal{P}}(\pi_{st}) \leq H_{\mathcal{P}}(\pi_{box}).$$

The goal of this section is to calculate $\langle H_{\mathcal{P}}(\pi_{box})\rangle_{\mathcal{P}}$; this is possible and easy to do thanks to hierarchical strucure of k-boxes, while should have

been very difficult with the Stable marriage algorithm. The following consideration are devoted to understand how to do this.

2.2.1 Evaluation of $\langle H_{\mathcal{P}}(\pi_{box})\rangle_{\mathcal{P}}$

Given an instance of Poisson points, we perform the algorithm.

Consider the preparatory step: after having married the points in a 0-box, we can obtain the following configurations of 0-boxes, described by the parameter q:

 if $h = 0$ then $q = -1$;

 if $h = 1$ then $q = 0$;

 if $h = 2$ then $q = 1$;

 if $h = 3$ then $q = 2$;

and so on.

The energy of the preparatory step is the sum of the energies coming from every 0-box, which can be maximized by: the number of marriages in a 0-box ($\#_{marr}(\text{0-box})$) multiplied by $\sqrt{2}$:

$$E_{prep} = \sum_{\text{0-box}} E(\text{0-box}) \lesssim \sum_{\text{0-box}} \#_{marr}(\text{0-box})\ \sqrt{2} \quad ;$$

this can be generalized for every k-step:

$$E(k) = \sum_{\text{(k+1)-box}} E(\text{(k+1)-box}) \lesssim \sum_{\text{(k+1)-box}} \#_{marr}(\text{(k+1)-box})\ \ 2^{k/2} \quad .$$

Now consider the 0-step; we see in fig. 2.3 (left) which are the possible 1-box configurations obtained joining two 0-boxes and marrying all possible pairs. We see that the number of marriages depends on the 0-boxes joined. In fig. 2.3 (right) we see the number of marriages in function of the parameter q of the joined 0-boxes.

We easily understand that:

- joining two 0-boxes with parameter q_1 and q_2 we obtain marriages if and only if $sign(q_1 \cdot q_2) = -1$;

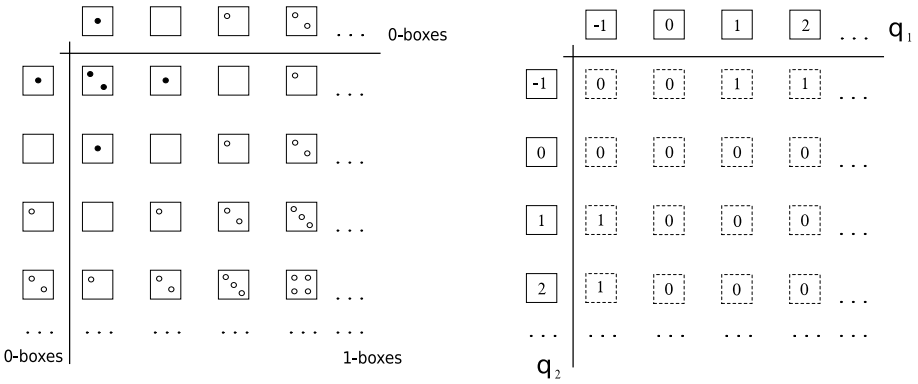

Figure 2.3: Left: the possible 1-box configurations obtained from the 0-step of the box algorithm. Right: the number of marriages in function of q_1 and q_2 at 0-step.

- the number of generated marriages is equal to $\min(|q_1|, |q_2|)$;

These two sentences are true at every k-step. Then the number of marriages of a $(k+1)$-box obtained joining two k-boxes, one with parameter q_1 and the other with parameter q_2, is:

$$\#_{marr}(\text{(k+1)-box}) = \min(|q_1|, |q_2|)\ \ \delta(sign(q_1 \cdot q_2), -1)$$

In conclusion we can write that:

$$\begin{aligned}
\langle E(k)\rangle_{\mathcal{P}} \ &\lesssim \sum_{\text{(k+1)-box}} \langle \#_{marr}(\text{(k+1)-box})\rangle_{\mathcal{P}}\ 2^{k/2} = \qquad (2.3)\\
&= \sum_{\text{(k+1)-box}} \langle\ \min(|q_1|, |q_2|)\ \ \delta(sign(q_1 \cdot q_2), -1)\ \rangle_{\mathcal{P}}\ 2^{k/2} = \\
&= \frac{N}{2^{k+1}}\ \langle\ \min(|q_1|, |q_2|)\ \ \delta(sign(q_1 \cdot q_2), -1)\ \rangle_{\mathcal{P}}\ 2^{k/2} = \\
&= \frac{N}{2^{k+1}} \sum_{q_1, q_2 = -2^k}^{N-2^k} p(q_1, k)\ p(q_2, k)\ \min(|q_1|, |q_2|)\ \ \delta(sign(q_1 \cdot q_2), -1)\ \ 2^{k/2}
\end{aligned}$$

where $p(q_i, k)$ is the probability that a k-box i has parameter q_i. Since $q_i = h_i - 2^k$ then $p(q_i, k) = p(h_i - 2^k, k)$; we calculate $p(h_i, k)$ that is the probability of finding h_i of M Poisson points in a k-box i.

Given M independent points, taken with uniform distibution on a set of measure V, the probability to find m points in a set of measure v is the binomial distribution:

$$p(m, v, M, V) = \binom{M}{m} \left(\frac{v}{V}\right)^m \left(1 - \frac{v}{V}\right)^{M-m}$$

that, for $m \gg 1$ and $M - m \gg 1$ is well described by a Gaussian distribution:

$$p(x, v, V, M) = \frac{1}{\sqrt{2\pi M \frac{v}{V}\left(1 - \frac{v}{V}\right)}} \exp\left[-\frac{\left(x - M\frac{v}{V}\right)^2}{2M\frac{v}{V}\left(1 - \frac{v}{V}\right)}\right].$$

Then for us: $m = h$, $v = 2^k$, $M = \rho N$ and $V = L^2 = N$:

$$p(h, k, N, \rho) = \binom{\rho N}{h} \left(\frac{2^k}{N}\right)^h \left(1 - \frac{2^k}{N}\right)^{\rho N - h}$$

and:

$$p(x, k, N, \rho) \sim \frac{1}{\sqrt{\rho 2^k}} \exp\left[-\frac{(x - \rho 2^k)^2}{2\rho 2^k}\right].$$

So the probability distribution for the parameter q, for a box at step k, is:

$$p(q, k, N, \rho) \sim \frac{1}{\sqrt{\rho 2^k}} \exp\left[-\frac{(q - (\rho - 1)2^k)^2}{2\rho 2^k}\right].$$

Now:

$$\langle E(k)\rangle_{\mathcal{P}} \lesssim \frac{N}{2^{k/2}} \int_D p(q_1, k, N, \rho) p(q_2, k, N, \rho) \min(|q_1|, |q_2|)$$

where the domain D is the light gray zone in fig. 2.4 and $p(q_1, k, N, \rho)p(q_2, k, N, \rho)$ is a two dimensional gaussian distribution centered in $\left((\rho - 1)2^k, (\rho - 1)2^k\right)$ and $\sigma = \sqrt{2\rho 2^k}$.

There will be two different behaviours depending on ρ:

- if $\rho \neq 1$, starting from $k \simeq -\frac{\ln|\rho-1|}{\ln 2}$, there will be pratically no overlap between the domain D and the gaussian distribution; then for $k \gtrsim -\frac{\ln|\rho-1|}{\ln 2}$ is $\langle E(k)\rangle_{\mathcal{P}} \sim 0$. Which means, by (2.2):

$$\langle H_{\mathcal{P}}(\pi_{box})\rangle_{\mathcal{P}} \sim N \qquad \text{for } N \to \infty\,;$$

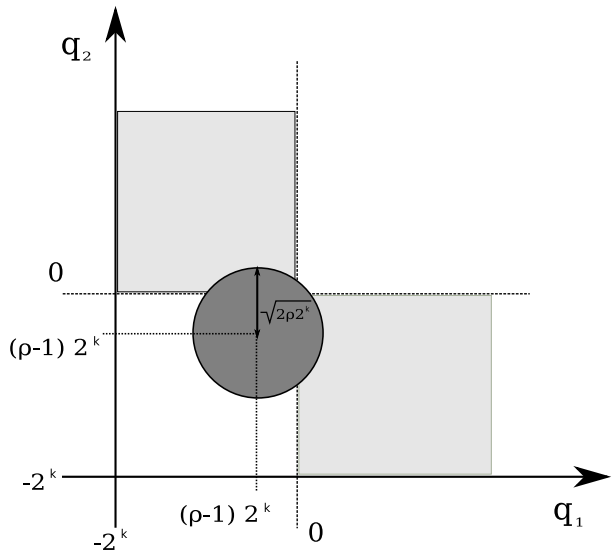

Figure 2.4: In light gray: the domain D. In dark gray: the points that fall in one σ of the gaussian distribution.

- if $\rho = 1$, for every value of k there is overlap between the domain D and the gaussian distribution; we can evaluate:

$$\int_D p(q_1, k, N, 1) p(q_2, k, N, 1) \min(|q_1|, |q_2|) \sim 2^{k/2} ,$$

and so substituing in (2.3) and for (2.2):

$$\langle H_{\mathcal{P}}(\pi_{box}) \rangle_{\mathcal{P}} \sim N \ln N \qquad \text{for } N \to \infty .$$

In conclusion the Box algorithm produces an upper bound to the mean value of the energy of the GPM obtained with the optimal marriage and with the Stable marriage; this upper bound is dependent on the density ρ:

$$\langle H_{\mathcal{P}}(\pi_{opt}, N) \rangle_{\mathcal{P}} \lesssim \langle H_{\mathcal{P}}(\pi_{st}, N) \rangle_{\mathcal{P}} \lesssim \begin{cases} N & \text{if } \rho \neq 1 \\ N \ln N & \text{if } \rho = 1 \end{cases} \quad \text{for } N \to \infty \quad (2.4)$$

2.3 Numerical simulations

In previous section we have introduced the Box algorithm, a heuristic for the GPM; we have seen by (2.4) that this heuristic produces an upper bound to the energy, which behaviour depends on the value of ρ: if $\rho \neq 1$,

the energy is bounded by N, if $\rho = 1$, the energy is bounded by $N \ln N$. We have also introduced the heuristic of Stable marriage algorithm.

We are interested to know if also the energy of the optimal marriage and of the Stable marriage present different behaviours depending on ρ, and if these behaviours are the same predicted by the Box algorithm. To do this, we have performed numerical simulations; we have used the Hungarian algorithm to obtain informations about $\langle H_{\mathcal{P}}(\pi_{opt}, N)\rangle_{\mathcal{P}}$ and the Stable marriage algorithm for $\langle H_{\mathcal{P}}(\pi_{st}, N)\rangle_{\mathcal{P}}$; these values have been obtained averaging the energies obtained from a sampling of 1.000 independent instances . With the Hungarian algorithm, which is $\mathcal{O}(N^3)$, we can arrive to investigate until the size $N = 1600$, which means a square of side $L = 40$; while with the Stable marriage algorithm, which is $\mathcal{O}(N^2)$, we can easily arrive to larger sizes: $N = L^2 = 512^2$. We present the results of our simulations.

First result. We present the results of a simulation in which we have set $\rho = 17/16$; we see in fig. 2.5 that, after initial strong finte-size corrections, growing the size N, $\frac{\langle H_{\mathcal{P}}(N)\rangle_{\mathcal{P}}}{N}$ becames a constant for both algorithms. This is in accord with the predictions of the heuristic, eq. (2.4).

Second result. We present the results of a simulation in which we have set $\rho = 1$; in fig. 2.6 we see that, for both algorithms, increasing size, $\frac{\langle H_{\mathcal{P}}(N)\rangle_{\mathcal{P}}}{N}$ grows. The heuristic predicts that, eq. (2.4), this cannot grow more than a logarithm.

Our data are well fitted by a function:

$$f(N) = a \ln N + b + c/N \, .$$

Since with the Stable marriage algorithm it is possible to reach with simulaions big sizes, we are sure enought that $\frac{\langle H_{\mathcal{P}}(N)\rangle_{\mathcal{P}}}{N}$ grows like a logarithm; on the other hand, for the difficulty to increase the size in simulations with the Hungarian algorithm, we cannot be sure of his behaviour. Fit values for both the algorithms are reported in table 2.1.

These results let us understand that for the GPM with $\rho = 1$ the energy is no more an extensive quantity, but this becomes super-extensive; this is surprising, but not unexpected; in fact it can motivated by fluctuations of Poisson point distribution: for $\rho \neq 1$ fluctuations are counterbalanced by the high number of Poisson points, while, for $\rho = 1$, these can be so strong to generate this behaviour.

Stable marriage		**Optimal marriage**	
a	0.0920 ± 0.0004	d	0.0343 ± 0.0009
b	0.565 ± 0.003	e	0.622 ± 0.006
c	-1.06 ± 0.06	f	-0.76 ± 0.07
reduced χ^2	0.260	reduced χ^2	0.522

Table 2.1: Values of fit parameters and of reduced χ^2 from data plotted in fig. 2.6.

These results shed some light on our model: we understand that this presents different behaviours depending on the density ρ; so we can say that this parameter has the same function that the temperature would have in a typical model of statistical mechanics; not only, we believe the model presents some criticality in $\rho = 1$, like suggested by the behaviour of the energy, then ρ is the critical parameter. The simulations that we will present in next chapters have been performed to test this criticality. We would also stress that ρ is not the only possible parameter for our model: it could be possible to introduce a temperature and then a Gibbs measure; since in the GPM we choose always the marriage with minimal energy, it is as if we would have set the temperature $T = 0$.

Third result. From these simulations we have also found the cumulant probability distribution for the energy at different sizes and fixed $\rho = 1$; we have found that this distribution is described by a Gumbel function:

$$\Lambda(x) = \exp\left(-e^{-x}\right).$$

Gumbel function is very particular [17]; it play a role similar to the one played by Gaussian function in central limit theorem. In fact, if $X_1, X_2, X_3, \ldots$ is a sequence of random variables i.i.d. with identical probability distribution and $M_n = \max(X_1, \ldots, X_n)$, then the probability distribution of M_n, for $n \to \infty$, is forced to be of only three possible kinds; one these is the Gumbel function.

Our fits, for different sizes, are plotted in fig. 2.7.

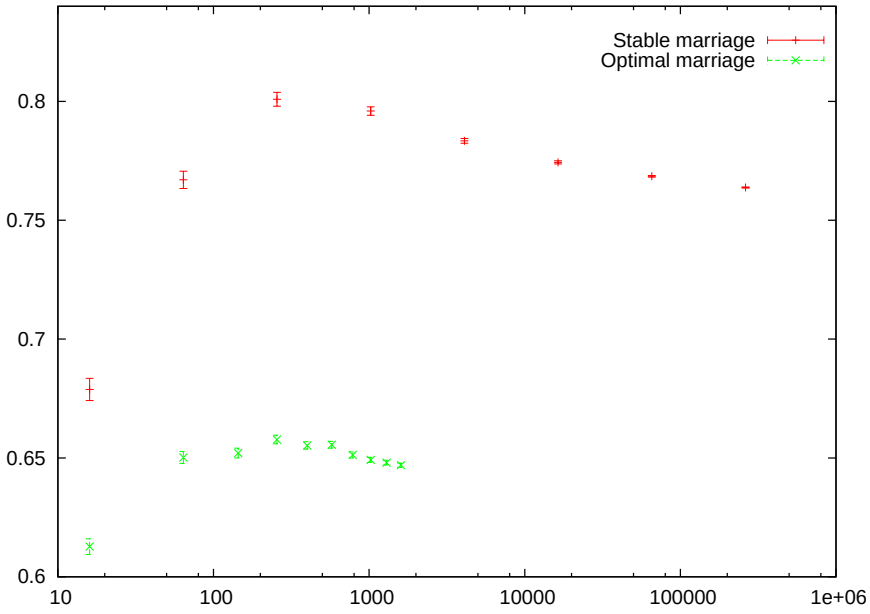

Figure 2.5: Plot of $\frac{\langle H_{\mathcal{P}}(N)\rangle_{\mathcal{P}}}{N}$ vs N for $\rho = 17/16$; these values have been obtained averaging the energies obtained from a sampling of 1.000 independent instances.

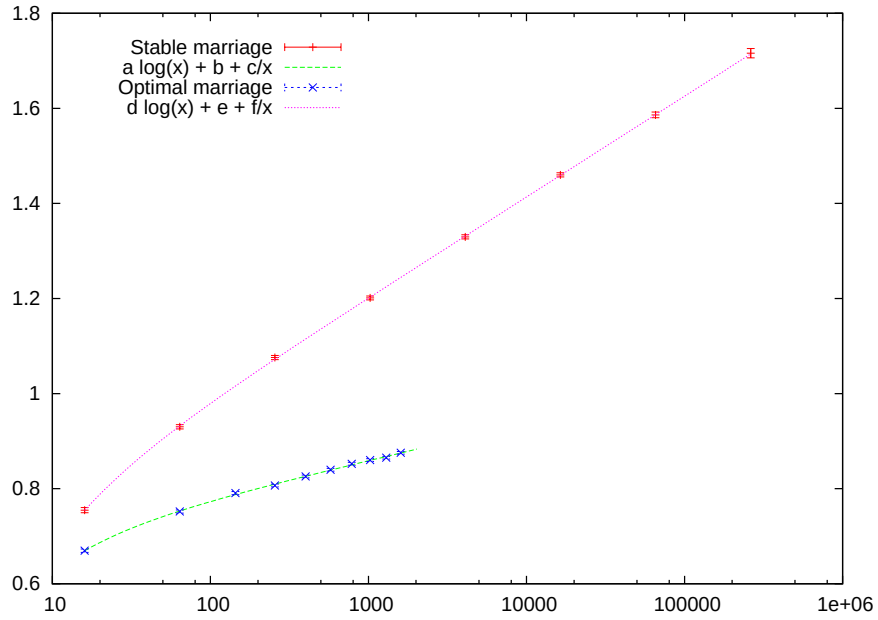

Figure 2.6: Plot of $\frac{\langle H_{\mathcal{P}}(N)\rangle_{\mathcal{P}}}{N}$ vs N for $\rho = 1$; these values have been obtained averaging the energies obtained from a sampling of 1.000 independent instances. The values of fit parameters and of the reduced χ^2 are reported in table 2.1.

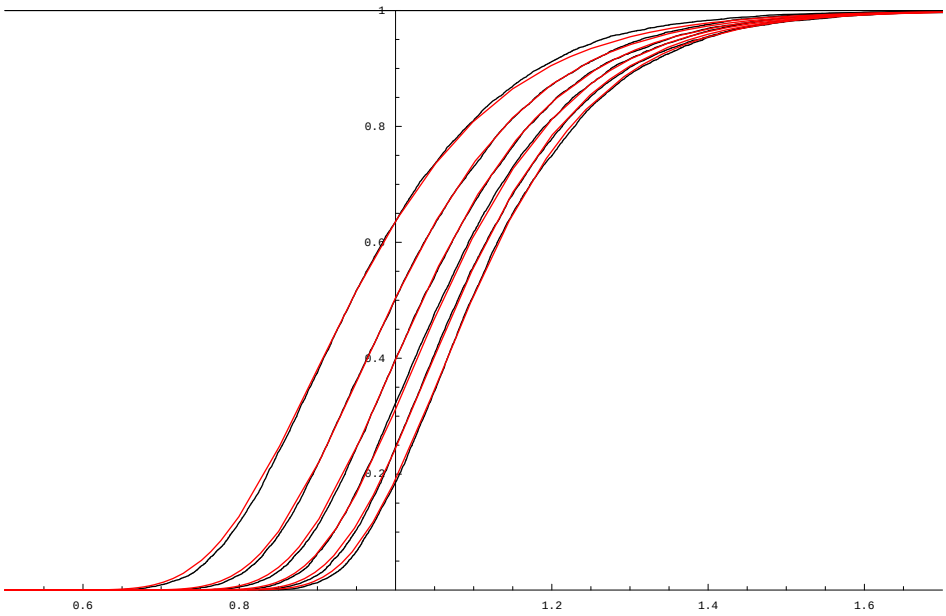

Figure 2.7: Plot of the cumulant distribution of the $H_{\mathcal{P}}(N)$ for $N = 8, 12, 16, 20, 24, 28$ (from left to right) in black, and the fits in red; distribution obtained from a sampling of 1.000 independent instances.

Chapter 3

Finite-size scaling

We have concluded the last section saying that we believe that GPM is critical in $\rho = 1$. The study of critical phenomena is one of the most exciting challanges of statistical mechanics. The behaviour of a system at the critical point is characterized by a diverging correlation length and cannot easily be approximated by considering small systems. Phase transitions are characterized by a non-analytic behaviour at the critical point of some observable. These non-analyticities are however observed only in the infinite-volume limit. If the system is finite, all thermodynamic functions are analytic in the thermodynamic parameters (like temperature or applied magnetic field in tipical models). However, even from a finite sample, it is possible to obtain many informations on the critical behaviour. Indeed, large but finite systems show a universal behaviour called finite-size scaling (FSS). The FSS is a very powerful method to extrapolate to the thermodynamic limit the results obtained from a finite sample, both in experiments and in numerical simulations. We refer to [18] for a complete tractation of this topic; in the following we will give a short introduction to FSS, giving emphasis to the aspects concerning our simulations.

3.1 Thermodynamic limit

We will describe FSS in the context of continuous (second-order) phase transitions in systems controlled by a single scalar parameter T which we assimilate to a temperature (for the GPM will be the density ρ). We assume the existence of a thermodynamic description of the system in a finite box Λ (e.g. a bounded subset of a discrete lattice where spin-like variables live): given any observable $\mathcal{O}$ we can compute its value on the thermody-

namic state determined by T and Λ as

$$\mathcal{O}_\Lambda(T) := \langle \mathcal{O} \rangle_\Lambda(T)$$

where $\langle \cdot \rangle_\Lambda(T)$ is the appropriate averaging. The infinite system is then understood in terms of the thermodynamic limit. Given an increasing sequence $\{\Lambda_n\}_n$ of boxes, the value $\mathcal{O}_\infty(T)$ of the observable in the infinite-volume system is given by:

$$\mathcal{O}_\infty(T) := \lim_{n \to \infty} \mathcal{O}_{\Lambda_n}(T)$$

Usually this limit exists for a wide class of $\mathcal{O}$ and taking arbitrary shapes for Λ_n.

The correlation length. The existence of the thermodynamic limit is tightly linked to the decay of correlation functions for local observables. In particular, in systems with short-range interactions, the (connected) correlation function

$$G_{\phi,\infty}(x) = \langle \phi(0)\phi(x) \rangle_\infty - \langle \phi(0) \rangle_\infty \langle \phi(x) \rangle_\infty$$

of a general local observable ϕ has an exponential decay. It is then possible to define a exponential correlation length $\xi_{\phi,\infty}$ for ϕ as:

$$\xi_{\phi,\infty} := - \lim_{|x| \to \infty} \frac{|x|}{\log |G_{\phi,\infty}(x)|}.$$

This is not the only possible definition of a correlation length in a infinite system; on the contrary, in finite volume does not exists a natural definition of correlation length and the one defined before cannot be generalized to finite volume. Then, in order to define consistently a finite system correlation length, we require that in the termodinamic limit this recover an infinite system correlation length.

Critical singularities. When $T \to T_c$ there are quantities $\mathcal{O}_\infty$ which behave as

$$\mathcal{O}_\infty(t) \sim |t|^{-x_\mathcal{O}} \quad \text{for} \quad t \to 0$$

where $t := (T - T_c)/T_c$ is the reduced temperature and where $\sim$ means that $|t|^{x_\mathcal{O}} \mathcal{O}_\infty(t)$ has a finite limit as $t \to 0$. Along with these diverging quantities it is possible to identify a distinguished local operator ϕ (the order parameter) for which the associated exponential correlation length $\xi_{\phi,\infty}$ diverges as

$$\xi_\infty \sim |t|^{-\nu}.$$

As we already remarked, in the finite systems all thermodynamic functions have an analytic dependence on control parameters which means that the interchange of the infinite-volume limit with the limit $t \to 0$ is in general not permitted:

$$\lim_{t\to 0}\lim_{\Lambda\to\infty} |t|^{x_\mathcal{O}}\mathcal{O}_\Lambda(t) \neq \lim_{\Lambda\to\infty}\lim_{t\to 0} |t|^{x_\mathcal{O}}\mathcal{O}_\Lambda(t) = 0$$

if, for example, $x_\mathcal{O} > 0$.

FSS theory predicts the asymptotic shape of the function $\mathcal{O}_\Lambda(t)$ when $\Lambda \to \infty$ and $t \to 0$ in a well-determined way.

3.2 Finite size scaling ansatz

A natural way of taking the infinite volume limit is to consider boxes of size L in all directions. Denote the corresponding averages with $\langle\cdot\rangle_L$. When $t \to 0$ there is a correlation length ξ which diverges. If L is large and if there are no other characteristic lengths of magnitude comparable to that of ξ or L we can write $\mathcal{O}_L(t)$ as a function of $\xi_\infty(t)$ and L:

$$\begin{aligned} \mathcal{O}_L(t) &\approx F_{\mathcal{O},0}(\xi_\infty(t), L) = \\ &= \xi_\infty(t)^{y_\mathcal{O}} F_{\mathcal{O},0}(1, L/\xi_\infty(t)) = \\ &= \xi_\infty(t)^{y_\mathcal{O}} F_{\mathcal{O},1}(L/\xi_\infty(t)) \end{aligned} \tag{3.1}$$

where $\approx$ means equality up to terms which are asymptotically negligible as $L, \xi_\infty \to \infty$. Indeed it is clear that, being ξ_∞ and L the only dimensionful quantities present, the function $F_{\mathcal{O},0}(x, y)$ must be a homogeneous function whose degree $y_\mathcal{O}$ can be determined through the limit $L \to \infty$ with ξ_∞ fixed:

$$\mathcal{O}_\infty(t) = \lim_{L\to\infty} \mathcal{O}_L(t) = \xi_\infty(t)^{y_\mathcal{O}} F_{\mathcal{O},1}(0) \sim |t|^{-\nu\, y_\mathcal{O}}$$

so we understand that $y_\mathcal{O} = x_\mathcal{O}/\nu$. With some assumptions on the existence of the limit for $F_{\mathcal{O},1}(z)$ when $|z| \to 0$.

Another way of rephrasing eq. (3.1) is

$$\mathcal{O}_L(t) \approx L^{x_\mathcal{O}/\nu} F_{\mathcal{O},2}(\xi_\infty(t)/L), \tag{3.2}$$

for $L \to \infty$ with $z := \xi_\infty(t)/L$ constant, where $F_{\mathcal{O},2}(z)$ has a finite limit for $z \to \infty$ and

$$F_{\mathcal{O},2}(z) \sim |z|^{x_\mathcal{O}/\nu} \quad \text{for} \quad z \to 0. \tag{3.3}$$

For a good finite-volume definition of correlation length ξ_L we obtain similarly

$$\xi_L(t) \approx L F_{\xi,2}(\xi_\infty(t)/L) \tag{3.4}$$

since in this case $x_\xi = \nu$. Moreover

$$\lim_{z \to 0_+} \frac{F_{\xi,2}(z)}{z} = 1. \tag{3.5}$$

3.2.1 Asymptotic FSS

The functional relation expressed by eq. (3.1) cannot be direclty used to analyze simulation (or experimental) data since usually the infinite-volume correlation length is an unknown quantity. A very common approach to overcome this problem is that of substituting the asymptotic expression of ξ_∞ as a function of t in (3.1) resulting in:

$$\mathcal{O}_L(t) \approx L^{x_\mathcal{O}/\nu} G_\mathcal{O}(tL^{1/\nu}). \tag{3.6}$$

The function $G_\mathcal{O}(z)$ is finite and non-vanishing in zero, and should satisfy

$$G_\mathcal{O}(z) \sim |z|^{-x_\mathcal{O}} \quad \text{for} \quad z \to \infty. \tag{3.7}$$

In eq. (3.6) only accessible quantities appear: t can be tuned by the experimentalist while $\mathcal{O}_L(t)$ is directly measurable. Even if the (infinite-volume) correlation length does not shows up explicitly it is always lurking in the background as witnessed by the presence of the related critical exponent ν. This form of FSS relies heavily on the knowledge of the critical temperature T_c (present in the definition of t).

Once we know T_c we can find the critical exponents though eq. (3.6) which says that there is a well defined functional dependence between $y = L^{-x_\mathcal{O}/\nu}\mathcal{O}_L$ and $x = tL^{1/\nu}$. We can then try to estimate values of $x_\mathcal{O}$ and ν such that the set of points (x_n, y_n) gathered from experiments collapse on a single curve. Of course this can approximately happen only for T near enough at T_c (for the scaling hypothesis to hold) and for L large enough (so that corrections to FSS are small): this is the critical region.

3.2.2 Correlation length FSS

Following e.g. [19], instead of replacing ξ_∞ with t in FSS relations we can proceed by inverting the functional relation expressed by eq. (3.4) to obtain

$$\frac{\xi_\infty(t)}{L} \approx F_{\xi,3}\left(\frac{\xi_L(t)}{L}\right) \tag{3.8}$$

Plugging this in eq. (3.1) we obtain a relationship which relates only quantities directly measurable in finite systems:

$$\mathcal{O}_L(t) \approx L^{x_\mathcal{O}/\nu} F_{\mathcal{O},3}\left(\frac{\xi_L(t)}{L}\right). \tag{3.9}$$

Taking the ratio of $\mathcal{O}_L$ at two different sizes L and αL we get

$$\frac{\mathcal{O}_{\alpha L}(t)}{\mathcal{O}_L(t)} \approx F_\mathcal{O}\left(\frac{\xi_L(t)}{L}\right) \tag{3.10}$$

where the (unknown) ratio $x_\mathcal{O}/\nu$ disappears.

The correlation length FSS is a good method to find the value of an observable $\mathcal{O}$ in the limit of $L \to \infty$. The method proceeds as follows. Make numerical simulations at numerous pairs (t, L) and $(t, \alpha L)$. Plot $\mathcal{O}_{\alpha L}(t)/\mathcal{O}_L(t)$ versus $\xi_L(t)/L$ using those points satisfying both $\xi_L(t) \geq$ some value ξ_{min} and $L \geq$ some value L_{min}. If all these points fall with a good accuracy on a single curve – thus verifying the ansatz (3.10) for $\xi_L(t) \geq \xi_{min}$ and $L \geq L_{min}$ – choose a smooth fitting function $F_\mathcal{O}$. Then, using the functions F_ξ and $F_\mathcal{O}$, extrapolate the pair $(\xi, \mathcal{O})$ successively from $L \to \alpha L \to \alpha^2 L \to \cdots \to \infty$.

3.3 Numerical simulations

We have seen that if a system verifies the FSS hypothesis, then there will be some observable $\mathcal{O}$ of the system which verifies the scaling relations described by eq. (3.6) or (3.10). In the following we will introduce a correlation function for the GPM, from which extrapolate a correlation length ξ; we will choose ξ as observable and then we will test the scaling relations.

Consider the GPM on the square: given an instance of Poisson points and found the optimal marriage, we can associate to every grid point with

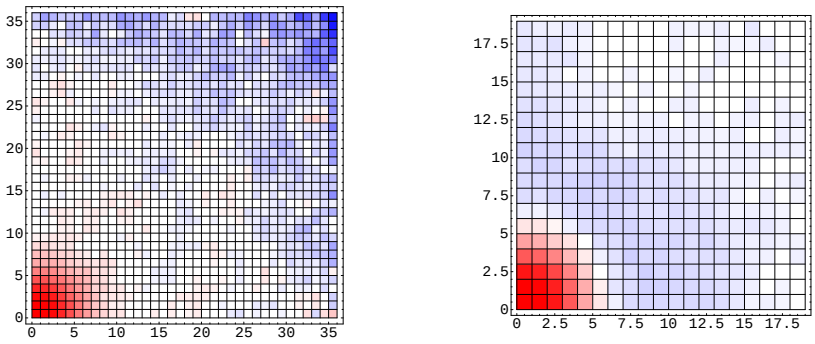

Figure 3.1: $G_{S,L}(\vec{0},\vec{r})$ (left) and $G_{T,L}(\vec{r})$ (right); red means positive correlation, blue negative correlation, white no correlation. These results have been obtained performing a sampling of 1000 independent instances of $N = 36^2$ grid points and $M = 1400$ Poisson points.

coordinates $\vec{x}$ a vector $\vec{\varphi}(\vec{x})$ with the tail in $\vec{x}$ and the tip in the married Poisson point. We introduce a finite size correlation function

$$G_{S,L}(\vec{x},\vec{y}) = \langle \frac{\vec{\varphi}(\vec{x})\cdot\vec{\varphi}(\vec{y})}{|\vec{\varphi}(\vec{x})||\vec{\varphi}(\vec{y})|}\rangle_{\mathcal{P}}. \tag{3.11}$$

Since now we have considered the GPM on a square; in the following we will also consider the same problem on a torus. We have introduced these new boundary conditions because this prevents our simulations to be affected from effects given to the border and then the correlation function becomes:

$$G_{T,L}(\vec{r}) = \sum_{\vec{x}} \langle \frac{\vec{\varphi}(\vec{x})\cdot\vec{\varphi}(\vec{x}+\vec{r})}{|\vec{\varphi}(\vec{x})||\vec{\varphi}(\vec{x}+\vec{r})|}\rangle_{\mathcal{P}}. \tag{3.12}$$

First of all we are interested to know if the behaviour of the correlation function depends on boundary conditions. In figure 3.1 we plot $G_{S,L}(\vec{0},\vec{r})$ (left) and $G_{T,L}(\vec{r})$ (right) obtained from simulations. We see that if we consider the square, there is a strong positive correlation near the origin, then, if we increase the distance, the correlation vanishes; only at the opposite corner there is a negative correlation, easily understood by geometrical reasons. While if we consider the torus, there is still a strong positive correlation near the origin, but this is rounded by a ring of negative correlation; increasing the distance the correlation vanishes.

Then we introduce a Wall-to-Wall correlation function, defined by

$$G_{W,L}(y) = \sum_{x} G_{T,L}(x,y)\,. \tag{3.13}$$

The correlation lengths that we will consider in the following are all extrapolated from the Wall-to-Wall correlation function, because it is easier to handle, since it is mono dimensional and defined on integers.

We can see in figure 3.2 typical Wall-to-Wall correlation functions obained with numerical simulation on a torus with 1600 grid points at different densities ρ. We see that, as expected from previous considerations, the correlation functions, after have reached a negative minimum value, present a right tail that go to zero. We have used two ways to extrapolate correlation lengths; the first one is to "cut" the right tail and fit the correlation functions with the following function:

$$f(x) = a + \exp(bx + c)$$

and then $\xi = 1/b$; the second one is to keep the tail and fit the correlation functions with:

$$f(x) = b\cosh\left[a(x - L/2)\right]\left[-1 + c\sin^2(\pi/2(x - L/2)/L)\right]$$

and then $\xi = 1/a$. We plot in figure 3.2 the fits obtained in the second way. The correlation lengths that have been used to obtain the results that are reported in the following had been obtained with fits of the first way; the error bars that will appear in following figures have been obtained propagating the errors of fit coefficients.

In conclusion of the previous section we have said that the density parameter played the role that in tipical models of statistical mechanics is played by the temperature; we had also argued that $\rho_c = 1$. Then for us the reduced temperature will be $t = \frac{\rho - \rho_c}{\rho_c} = \rho - 1$.

Asymptotic FSS. In this simulation we have tested if our model verifies the scaling ansatz (3.6). We choose as observable $\mathcal{O}_L$ the correlation length ξ_L, then $x_\xi = \nu$; then eq. (3.6) becomes:

$$\frac{\xi_L(t)}{L} \approx G_\xi(tL^{1/\nu}) \,. \tag{3.14}$$

Our method has been the following: we have performed numerical simulations at different sizes L and different densities ρ, and we have extrapolated the correlation length $\xi_L(t)$, as explained before. Then if it is true that the GPM is critical in $\rho = 1$, there must be a value of ν such that the coulples of points $(\xi_L(t)/L, tL^{1/\nu})$ collapse on a single curve. We present our results for $\nu = 3/4, 5/4, 7/4$ and $9/4$ in figures 3.3, 3.4, 3.5 and

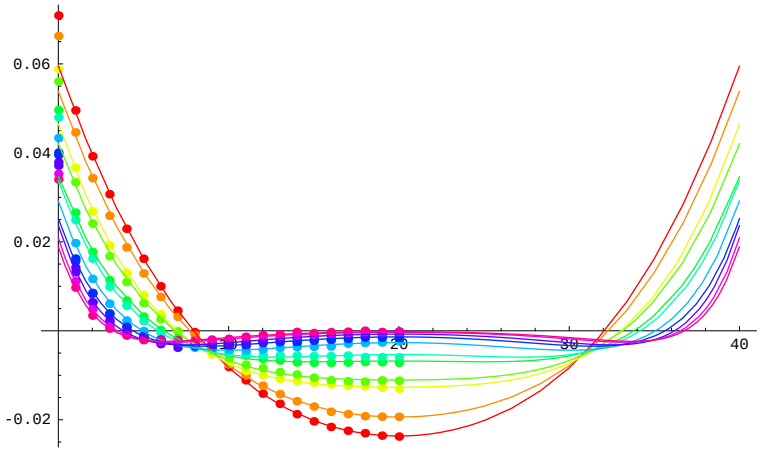

Figure 3.2: Plot of $G_{W,L}(x)$ obtained performing a sampling of 1000 independent instances on a torus with 1600 grid points and with the following Poisson points: 1612, 1620, 1632, 1640, 1652, 1660, 1680, 1700, 1720, 1740, 1760, from red to purple.

3.6. We see that for $\nu = 5/4$, or values near to this, the points stay with a good accuracy on a curve, while for $\nu = 7/4$, or greater, and $\nu = 3/4$ or smaller, the points are scattered.

Correlation length FSS. In this simulaiton we have tested if our model verifies the scaling ansatz (3.10). Once again we have chosen as observable $\mathcal{O}$ the correlation length ξ, and as parameter $\alpha = 2$; then (3.10) becames:

$$\frac{\xi_{2L}(t)}{\xi_L(t)} \approx F_\xi\left(\frac{\xi_L(t)}{L}\right) . \tag{3.15}$$

We have performed numerical simulations at $L = 20, 22$ and we have extrapolated the correlation length. Plotting (fig 3.7) $\xi_{2L}(t)/\xi_L(t)$ versus $\xi_L(t)/L$, we see that the points fall with a good accuracy on a curve. We have also found that the points are well fitted by a curve:

$$F_\xi(x) = 1 + a \exp(b/x) \tag{3.16}$$

and fit parameters are reported in table 3.1.

The choose to use this function is partially motivated by the theory, which tells us that $F(x) \to 1$ exponentially fast as $x \to 0$.

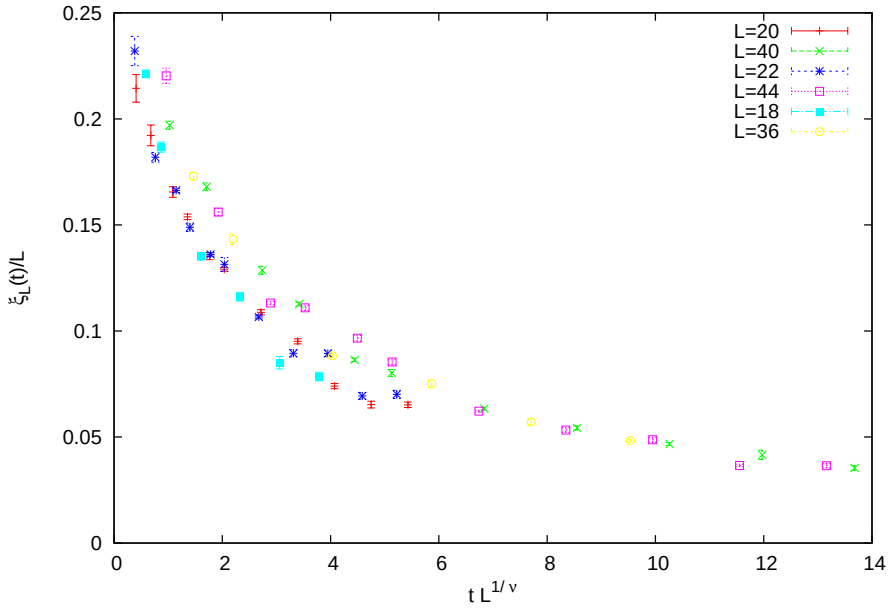

Figure 3.3: Plot of $\xi_L(t)/L$ versus $tL^{1/\nu}$, with $\nu = 3/4$.

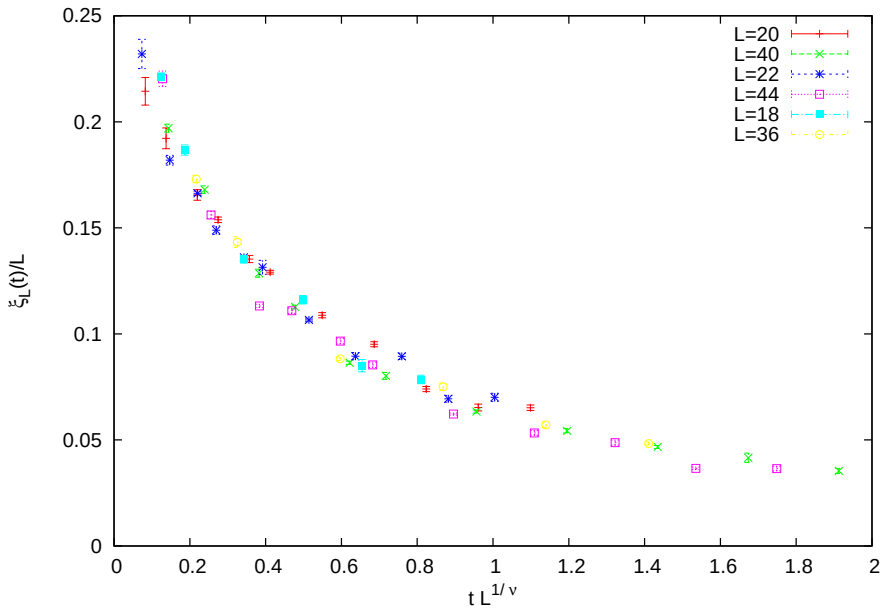

Figure 3.4: Plot of $\xi_L(t)/L$ versus $tL^{1/\nu}$, with $\nu = 5/4$.

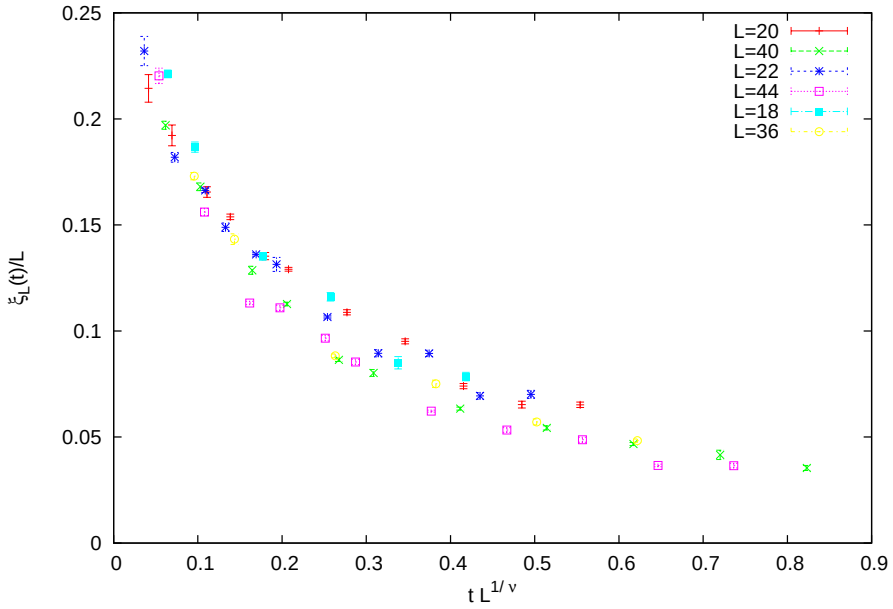

Figure 3.5: Plot of $\xi_L(t)/L$ versus $tL^{1/\nu}$, with $\nu = 7/4$.

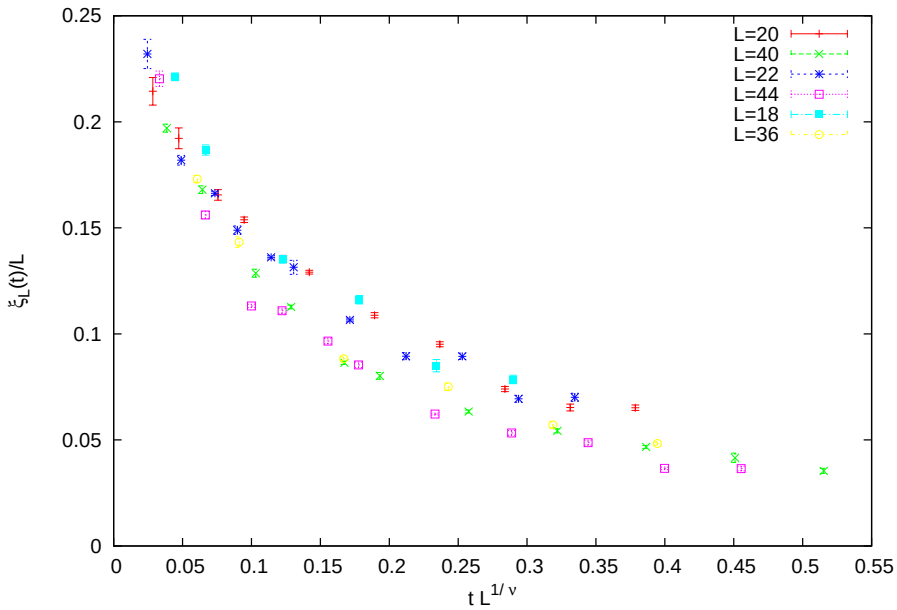

Figure 3.6: Plot of $\xi_L(t)/L$ versus $tL^{1/\nu}$, with $\nu = 9/4$.

Fit parameters	
a	3.7266 ± 0.3919
b	-0.318109 ± 0.01838
reduced χ^2	0.0022

Table 3.1: Values of fit parameters and of reduced χ^2 obtained fitting data plotted in fig. 3.7 with the function $F_{\tilde{\xi}}(x) = 1 + a \exp(b/x)$.

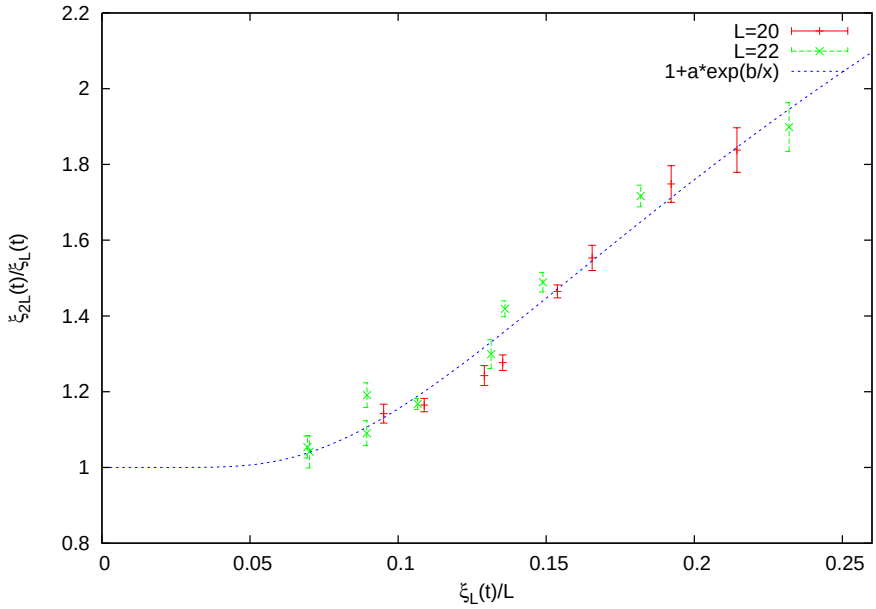

Figure 3.7: Plot of $\xi_{2L}(t)/\xi_L(t)$ versus $\xi_L(t)/L$ for $L = 20, 22$; the solid line is the fit with a curve $F_{\tilde{\xi}}(x) = 1 + a \exp(b/x)$.

Chapter 4

Test of conformal invariance of spanning trees in GPM

In this chapter we will show that with the Hungarian algorithm it is possible to generate in a natural way spanning tree on the complete graph with vertices the grid points; we will test the conformal invariance for this ensemble of spanning trees.

4.1 Conformal maps

We define a domain as an open connected subset of the complex plane. We call a domain simply connected if it contains no holes. More precisely, a domain is simply connected if its complement in the complex plane is connected or, equivalently, if every closed curve in the domain can be contracted continuously to a single point of the domain.

A conformal map f of a simply connected domain $D \neq \mathbb{C}$ onto another simply connected domain $D' \neq \mathbb{C}$ is a one-to-one map which preserves angles. That is, if γ_0 and γ_1 are two curves in D which intersect at a certain angle, then their images $f \circ \gamma_0$ and $f \circ \gamma_1$ must intersect at the same angle. In practice this means that a conformal map $f : D \to D'$ is an injective and analytic function on D, which has nonzero derivative everywhere on D. It has an inverse f^{-1} which is also conformal.

A foundamental theorem about these conformal maps is the Riemann mapping theorem, which tells us that any simply connected domain D can be mapped conformally onto the open unit disk $\mathbb{D} = \{z \in \mathbb{C} : |z| < 1\}$. Note that the theorem says nothing about the behaviour of the map at the boundary ∂D.

Theorem 3 (Riemann mapping theorem)**.** *Let $D \neq \mathbb{C}$ be a simply connected domain in $\mathbb{C}$. Then there is a conformal map of D onto the open unit disk $\mathbb{D}$.*

The conformal map of a domain D onto $\mathbb{D}$ is unique up to composition with a conformal map of the unit disk into itself. Therefore, the Riemann mapping theorem together with the following theorem on the conformal maps of the unit disk into itself provide the basis for the theory of conformal maps.

Theorem 4. *The conformal maps of the open unit disk $\mathbb{D}$ into itself are precisely the transformations of the form*

$$f(z) = e^{i\phi}\frac{z-a}{1-\bar{a}z} \qquad |z| < 1$$

where a is complex, $|a| < 1$, and $0 \leq \phi \leq 2\pi$.

It follows from this theorem that the map $f : D \to \mathbb{D}$ is determined uniquely if we specify three real parameters. For example, one commonly specifies $f(z) = 0$ and $f'(z) > 0$ (which makes sense when $f'(z)$ is real and positive) at some specific point $z \in D$, to make the map unique.

Using the Riemann mapping theorem, we can also study conformal maps between two simply connected domains $D, D' \neq \mathbb{C}$ in the complex plane. A conformal map of D onto D' is easily defined through the conformal map of D onto $\mathbb{D}$, and the inverse of the map of D' onto $\mathbb{D}$. Again, the map is unique if we specify three real parameters. For example, if we fix two points $z \in D$, $w \in D'$, then there is a unique conformal map f of D onto D' with $f(z) = w$ and $f'(z) > 0$. Another way commonly used to specify a map uniquely is the following. Fix three distinct points z_1, z_2, z_3 ordered counter-clockwise on the boundary of D, and three distinct points w_1, w_2, w_3, ordered similarly on the boundary of D' . Then there is a unique conformal map f of D onto D' with $f(z_i) = w_i$, $i = 1, 2, 3$.

A domain that we will often use in the following is the complex upper half-plane $\mathbb{H} = \{z \in \mathbb{C} : \mathrm{Im}(z) > 0\}$. Our first observation is that any simply connected domain can be mapped conformally onto $\mathbb{H}$. This follows from the Riemann mapping theorem, and the fact that the map $f(w) = i(1+w)/(1-w)$ is a standard conformal map of $\mathbb{D}$ onto $\mathbb{H}$. We can also go back from the upper half-plane to the unit disk by using the inverse map $f^{-1}(z) = (z-i)/(z+i)$.

Conformal maps of simply connected domains onto the upper half-plane are unique up to composition with the conformal maps of the upper

half-plane into itself. The form of these maps is given by the following theorem.

Theorem 5. *The conformal maps of the upper half-plane* $\mathbb{H}$ *into itself are precisely the (fractional linear or Möbius) transformations*

$$f(z) = \frac{az+b}{cz+d} \qquad Im(z) > 0$$

where a, b, c *and* d *are real numbers satisfying* $ad - bc > 0$.

4.1.1 Schwarz-Christoffel trasformation

In this section we will introduce the Schwarz-Christoffel formula for constructing a conformal map from the upper half-plane $\mathbb{H}$ onto a region G bounded by a polygonal curve.

Theorem 6 (Schwarz-Christoffel formula)**.** *Let* P *a polygon in the complex plane* $\mathbb{C}$ *with vertices* $w_1, w_2, \ldots, w_n$ *and exterior angles* $\alpha_1, \alpha_2, \ldots, \alpha_n$*, where* $-\pi < \alpha_k < \pi$*. There exists a conformal map* f *from the upper half-plane* $\mathbb{H}$ *onto* G *that satisfies the boundary conditions:*

$$w_k = f(x_k) \qquad for\ \ k = 1, 2, \ldots, n-1 \qquad and \quad w_n = f(\infty)$$

where x_i *are real and ordered:* $x_1 < x_2 < \cdots < x_{n-1} < \infty$*. The derivative* $f'(z)$ *is*

$$f'(z) = A\ (z - x_1)^{-\alpha_1/\pi}(z - x_2)^{-\alpha_2/\pi} \ldots (z - x_{n-1})^{-\alpha_{n-1}/\pi}$$

and the function $f(z)$ *can be expressed as an indefinite integral*

$$f(z) = B + A \int (z - x_1)^{-\alpha_1/\pi}(z - x_2)^{-\alpha_2/\pi} \ldots (z - x_{n-1})^{-\alpha_{n-1}/\pi} \mathrm{d}z$$

where A *and* B *are suitably chosen constants.*

We give a clarifying example of a conformal map obtained by the Schwarz-Christoffel formula; this example will also be useful in the next chapter. We use the Schwarz-Christoffel formula to verify that

$$f(z) = \sqrt{z^2 - 1}$$

maps $\mathbb{H}$ onto $\mathbb{H}$ slit along the line segment from $w = 0$ to $w = i$. We choose $x_1 = -1, x_2 = 0, x_3 = 1$, $w_1 = -d, w_2 = i, w_3 = d$ and $\alpha_1, \alpha_2, \alpha_3$ as in figure (4.1); then, from the Schwarz-Christoffel formula, we obtain

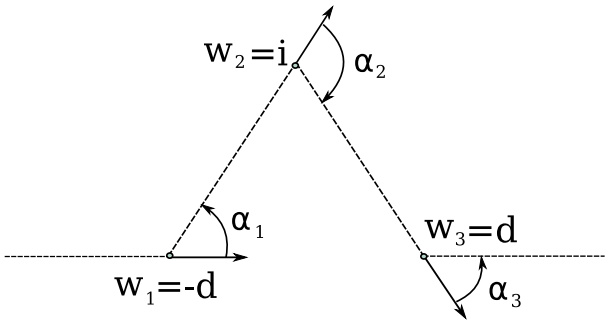

Figure 4.1: The points $w_1 = -d, w_2 = i, w_3 = d$ and angles $\alpha_1, \alpha_2, \alpha_3$.

$$f'(z) = A\ (z+1)^{-\alpha_1/\pi}(z)^{-\alpha_2/\pi}(z-1)^{-\alpha_3/\pi}.$$

Now, if we let $d \to 0$, we have $w_1 \to 0$, $w_3 \to 0$ and $\alpha_1 \to \pi/2$, $\alpha_2 \to -\pi$ and $\alpha_3 \to \pi/2$. Then the limiting formula is

$$f'(z) = A\frac{z}{\sqrt{z^2-1}}\,.$$

Integrating we have:

$$f(z) = B + A\sqrt{z^2-1}\,.$$

Imposing that $f(\pm 1) = 0$ and $f(0) = i$, we find that:

$$f(z) = \sqrt{z^2-1}\,.$$

We easily find also that the inverse function that maps $\mathbb{H}$ slit along the line segment from $z = 0$ to $z = i$ onto $\mathbb{H}$ is:

$$f^{-1}(z) = \sqrt{z^2+1}. \tag{4.1}$$

We present, wihout proof, other maps that we will use in the following; the domains that we consider are: the circle $\mathbb{D}$, the upper half-plane $\mathbb{H}$ and the square $S = [0,1] \times [0,i]$. The maps between these domains are:

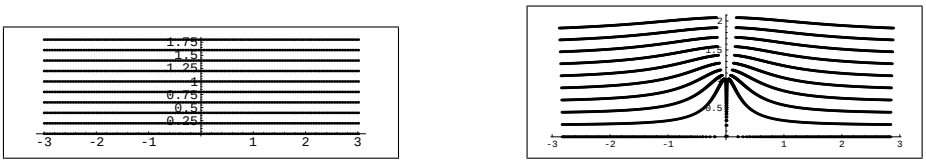

Figure 4.2: Left: Straight lines on $\mathbb{H}$. Right: Straight lines on $\mathbb{H}$ mapped to $\mathbb{H}$ slit along the line segment from $w = 0$ to $w = i$ with the function $f(z) = \sqrt{z^2 - 1}$.

$$
\begin{aligned}
f_{\mathbb{D}\to\mathbb{H}}(z) &= i(1+z)/(1-z) && (4.2)\\
f_{\mathbb{H}\to\mathbb{D}}(z) &= (z-i)/(z+i) && (4.3)\\
f_{\mathbb{H}\to S}(z) &= \frac{F\left(\ \arcsin\left(\sqrt{z}\right)\ \middle|\ \text{-1}\ \right)}{K(-1)} && (4.4)\\
f_{S\to\mathbb{H}}(z) &= \operatorname{sn}\left(z\,K(-1)\middle|-1\right) && (4.5)\\
f_{\mathbb{D}\to S}(z) &= \frac{F\left(\ \arcsin\left(\sqrt{i\frac{1+z}{1-z}}\right)\ \middle|\ \text{-1}\ \right)}{K(-1)} && (4.6)\\
f_{S\to\mathbb{D}}(z) &= \frac{\operatorname{sn}\left(z\,K(-1)\middle|-1\right)-i}{\operatorname{sn}\left(z\,K(-1)\middle|-1\right)+i} && (4.7)
\end{aligned}
$$

where $F(z|m)$ is the elliptic integral of the first kind, $K(m)$ is the complete elliptic integral of the first kind and $\operatorname{sn}(z|k)$ is a Jacobi elliptic function, see [32].

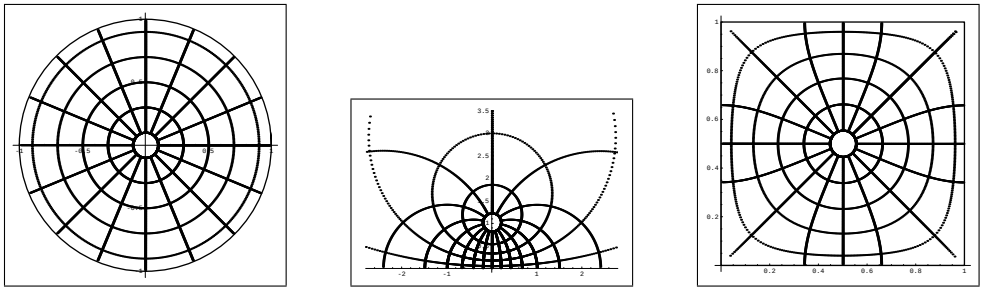

Figure 4.3: Left: The circle $\mathbb{D}$. Center: $\mathbb{D}$ mapped into $\mathbb{H}$ with $f_{\mathbb{D}\to\mathbb{H}}(z)$. Right: $\mathbb{D}$ mapped into the square with $f_{\mathbb{D}\to S}(z)$.

4.2 Special gauges and spanning trees

In this section we come back to the assignment problem; we introduce the so called *special gauges* in order to show how we can associate to every instance of the GPM a spanning trees on the complete graph with vertices the grid points.

Theorem 7. *Given an instance ϵ of assignment problem, and a column j, it is always possible to perform a Hungarian gauge transformation such that in the gauged matrix ϵ' all the columns $j' \neq j$ have at least two zeroes. Moreover, if the instance is non-degenerate, there is exactly one zero in column j and two zeroes in all the other columns, and the graph of zeroes Z is a spanning tree on $\mathcal{K}_{N,N}$.*

Given a proper gauge ϵ we call π_{opt} the optimal assignment. Up to a relabeling of the columns, we can assume that $j = 1$ and that π_{opt} is the identity permutation. We will call $H_1 = H_\epsilon(\pi_{opt})$.

For each $i \in [N]$ and $i \neq 1$, we define π_i the optimal assignment in the subensemble of permutations such that $\pi(i) = 1$ and then $H_i = H_\epsilon(\pi_i)$.

Consider the following gauge:

$$\begin{cases} \lambda_i = \epsilon_{i1} + H_1 - H_i \\ \mu_j = \epsilon_{jj} - \lambda_j \end{cases} ;$$

the gauged matrix ϵ' will have the following properties:

$$\begin{aligned} \epsilon'_{ii} &= 0 \qquad \forall i \in [N] \, ; \\ \epsilon'_{i1} &= H_i - H_1 \quad \forall i \in [N] \, . \end{aligned}$$

It is possible to prove [20] that ϵ' is a proper gauge; then ϵ' is hungarian.

In order to prove that ϵ' has at least two zeroes per column $i \geq 2$, consider the minor of ϵ' obtained by deleting column 1 and row i; we have a matrix with non-negative entries, that contains an assignment of zero cost (since $H_i = H_\epsilon(\pi_i) = H_{\epsilon'}(\pi_i) + H_1$ then $H_{\epsilon'}(\pi_i) = H_i - H_1$; since $\epsilon_{i\ \pi_i(i)} = \epsilon_{i1} = H_i - H_1$ then $\epsilon'_{j\ \pi_i(j)} = 0\ \forall j \neq 1$), and this implies that every column has at least one zero entry. This statement says nothing on columns $j \neq i$, where one still has the entry $\epsilon'_{jj} = 0$ by construction, but the entry ϵ_{ii} is not in the minor, so there must be another zero in the same column.

If the instance is not degenerate, the set Z_{min} has cardinality N and, for any hungarian gauge, the graph Z has no loops. As we have proven that our gauge has at least $2N - 1$ edges, and a loop-free subgraph of a graph

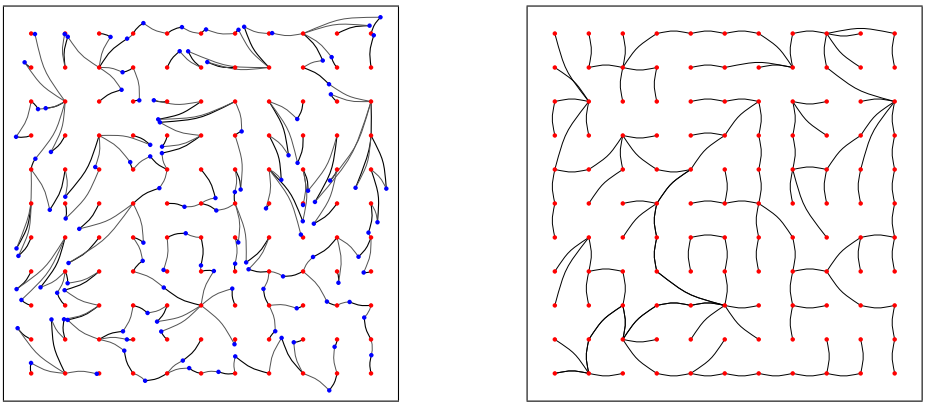

Figure 4.4: Left: the spanning tree on the complete bipartite graph $\mathcal{G} \cup \mathcal{P}$. Right: the spanning tree on the complete graph $\mathcal{G}$ obtained from the previous one.

with $2N$ sites has at most $2N - 1$ edges (in this case being a spanning tree) for the Euler formula (1.2), also the final statement of the theorem follows. □

We will call the gauge ϵ' obtained in the theorem *special gauge*. This theorem is true in general for the assignment problem, and then we can consider it applied to the GPM; in that case the bipartite graph $\mathcal{K}_{N,N} = \mathcal{G} \cup \mathcal{P}$; then generating an instance of Poisson points, associating it the matrix ϵ and finding the special gauge ϵ', we generate a spanning tree on the complete bipartite graph $\mathcal{G} \cup \mathcal{P}$. We see an example in figure 4.4 (Left). The fact that every column $i \neq j$ of the matrix ϵ' has two zeros implies that every Poisson point $i \neq j$ has exactly two incident edges that we will call (a_i, i) and (b_i, i), where a_i, b_i are grid points. We delete every Poisson point $i \neq j$ and his two incident edges, and we replace them with the edge (a_i, b_i); we delete also the Poisson point j with his edge, and then we obtain a spanning tree on the grid points, as we see in figure 4.4 (Right).

We have implemented an algorithm that generates an instance of Poisson points and, using repeatedly the Hungarian algorithm, finds the special gauge and then the spanning tree. We note that, for what said before, that the spanning tree generated depends on the choice of the Poisson point j; since Poisson points are taken with random distribution on the square, the choice of a given j does not introduce an arbitraty act in the sampling of the trees; this would not have been true if we had to choose a grid point j.

It is possible to see, from the distribution of the lengths of the edges of the trees obtained by the sampling, that it is hardly probable to generate trees with long edges; this means that, also if the trees generated by the GPM are not planar, the violation to planarity are rare events, and then this ensemble of trees is not very different from an ensemble of planar trees; apart little corrections, they are in the same universality class.

We will also stress the fact that we have to use repeatedly the Hungarian algorithm, N times for every instance, to generate the spanning tree; this implies that the computational complexity of the algorithm that generates spanning trees is $\mathcal{O}(N^4 = L^8)$.

In the following section we will deal with questions as: which is the probability measure for the spanning trees generated with the special gauges? Is this measure conformally invariant?

4.3 Test on conformal invariance of spanning trees

4.3.1 Introduction

One of the main goals of both probability theory and statistical physics is to understand the asymptotic behavior of random systems when the number of microscopic random inputs goes to infinity. O. Schramm [21], in 1999, explained:

> It is often the case that grid-based probabilistic model should be considered as a mere substitute, or semplification, of a continous process. There are definite advantages for working in the discrete setting, where unpleasant technicalities can frequently be avoided, simulations are possible, and the setup is easier to comprehend. On the other hand, one is often required to pay some price for the simplification. When we adopt the grid-based world, we sacrifice rotational or conformal symmetries that the continous model can enjoy, and often have to accept some arbitrarines in the formulation of the model [...]. Understanding the connections between grid-based models and continous processes is a project of foundamental importance, and so far has only limited success.

One resonable way to define a continous process, is by taking a scaling limit of a grid process. This means making sense of the limit of a sequence of grid processes on finer and finer grids.

In his work Schramm considered the Loop Erased Random Walk (LERW) on a domain $D \cap \delta\mathbb{Z}^2$ (a LERW from $a \in D$ to $b \in D$ is a random simple curve joining a to b obtained by erasing the loops in chronological order from a simple random walk started at a and stopped upon hitting b); he defined a measure $\mu_\delta(D, a, b)$ supported on the LERW on the domain $D \cap \delta\mathbb{Z}^2$ and a scaling limit for $\delta \to 0$. Then he proved that the scaling limit measure $\mu(D, a, b)$ is defined on simple paths in D from a to b. Not only, he conjectured that the limiting measure was conformally invariant; conformal invariance means that: consider two domains D and D' and a conformal map $f : D \to D'$, if $a, b \in D$ then $f(a), f(b) \in D'$. The measure μ on simple curves on D induces a measure, called $f * \mu$ supported on simple curves on D'; the conformal invariance property states that this is the same as the measure which would be obtained as the continuum limit of lattice curves from $f(a)$ to $f(b)$ in D'. That is:

$$(f * \mu)(D, a, b) = \mu(D', f(a), f(b)).$$

This conjecture was proved two years after in [22]. Conformal invariance is a very useful property, because, by the Riemann mapping theorem, if we know the measure for one simply connected domain D, we know it for all simply connected domains.

Now we can consider spanning trees; given a graph and a measure on spanning trees of the graph, we can sample spanning trees. For example:

- Uniform Spanning Trees (UST): a UST in a finite, connected graph G is a sample from the uniform probability measure on spanning trees of G;

- Minimal Spanning Trees (MST): the MST is formed by assigning uniformly random weights to the edges of the graph, and picking the spanning tree which minimizes the total weight.

If the reader is interest to a study of conformal invariance of this ensembles of trees, we refer to [23].

Since UST are strictly related by LERW, as proved by D. Wilson [24] with his algorithm, has been proved that is possible to define a scaling limit for UST and that they are conformally invariant.

4.3.2 Test on conformal invariance

In [25] D. Wilson proposed a test of conformal invariance for spanning trees; to prove the good quality of his test, he performed it on UST and,

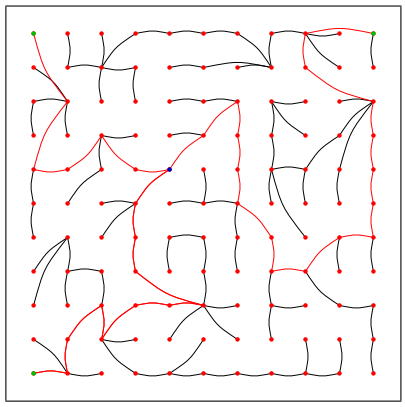

Figure 4.5: In red the path joining the green points at the corners of the square; the blue point is the triple point.

as expected, could not exclude their conformal invariance. Starting from this result, he performed the test on the yet unproved MST and excluded that they could be conformally invariant. We have used this test to try to understand if the spanning trees generated with the GPM can be conformally invariant, as conjectured by us.

Consider a tree; chosen three vertices of the tree, find the three paths joining this points; since we deal with a tree, the union of these paths contains no loops and, not rigorously speaking, form a kind of "Y"; there is also only one point belonging at the same time to the three paths, this is called "triple point".

Consider then a spanning tree generated by the GPM and, as proposed by D. Wilson, choose the three points at the corners of the square (the green points in figure 4.5) and call T the triple point (the blue point in figure 4.5). Consider also the map

$$f_{S\to\mathbb{D}}(z) = \frac{3i\mathrm{sn}\left(z\,K(-1)|-1\right)+\sqrt{3}}{\sqrt{3}-3i\mathrm{sn}\left(z\,K(-1)|-1\right)} \tag{4.8}$$

that maps the square to the disk $\mathbb{D}$, as we see in figure 4.6.

The test is the following: if spanning trees were conformally invariant, than the image of spanning trees on the disk $\mathbb{D}$ would be isotropic; if this was, then T, $T\,e^{\pi i/3}$ and $T\,e^{2\pi i/3}$ would be equidistribuited.

We applied this test to trees generated by GPM. In order to do that, we have found the distribution of the triple point in the square of side $L = 16$

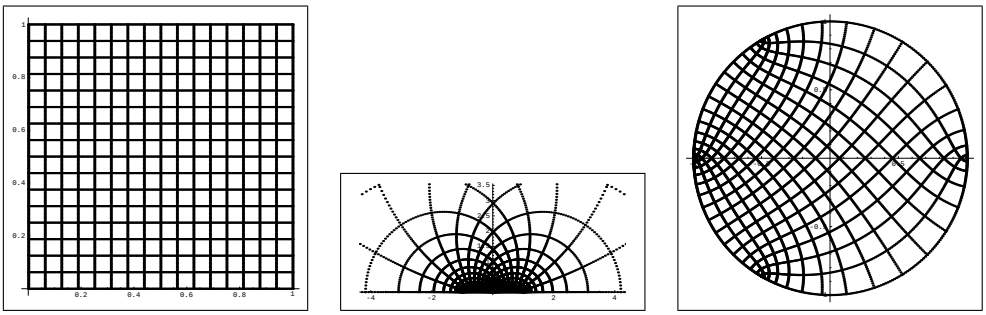

Figure 4.6: Left: a grid on a square. Center: the grid mapped into $\mathbb{H}$. Right: the grid mapped into the disk $\mathbb{D}$ with $f_{S\to\mathbb{D}}(z)$.

averaged over 28.000 independent instances and we have mapped it into the disk with $f_{S\to\mathbb{D}}(z)$ of eq. (4.8), as plotted in figure 4.7; then we obtained the difference of this distribution and the the same distribution rotated of 120°; we have plotted this in figure 4.8: red means positive difference, blu negative difference and white no difference. From this result it is difficult to conclude if there is or not conformal invariance.

We underline that we have arrived only at $L = 16$; it could be an interesting perspective to perform simulations at larger size, but this would need strong efforts in computational time, since, as said before, the complexity of the algorithm that generates spanning trees is $\mathcal{O}(N^4 = L^8)$.

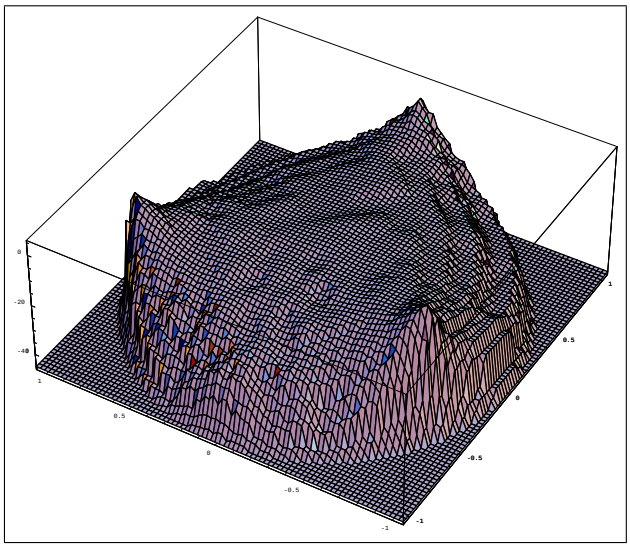

Figure 4.7: The distribution of the triple point, obtained from a sampling of 28.000 instances of Poisson points, mapped in the circle.

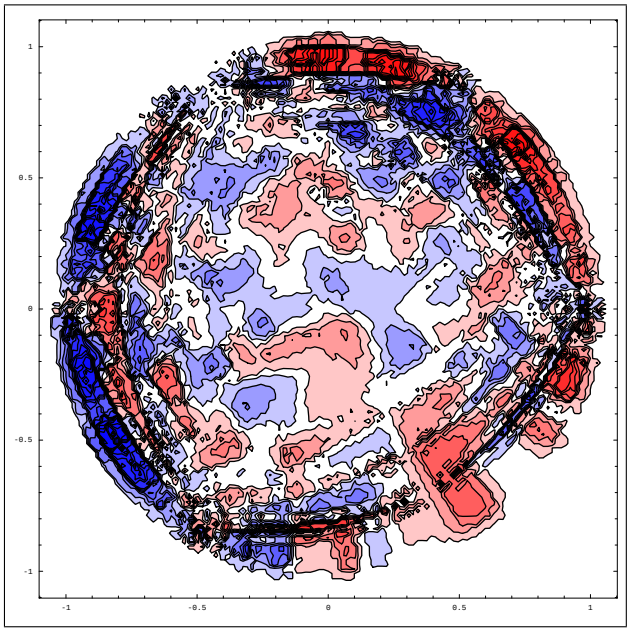

Figure 4.8: The difference between the distribution of the triple point mapped into the circle, figure 4.7, and the same rotated of 120°; red means positive difference, blu negative difference and white no difference.

Chapter 5

Connection between GPM and SLE

In this chapter we will give a short introduction to Stochastic Loewner Evolution (SLE), a mathematical tool that is conjectured to describe the scaling limit of curves generated by models of statistical mechanics at the critical point; recently, some efforts have been also done to relate minimal paths in two dimensional disordered systems and SLE processes, see for example the boundary walls in Ising Spin Glasses [26] [27]. We will see that also the GPM, at the critical value $\rho = 1$, generates curves; we will test if these curves can be described by a SLE.

5.1 Stochastic Loewner Evolution

In this section we introduce Stochastic Loewner Evolution, following the rewievs of Cardy [28], Nienhuis [29] and Gruzberg [30].

5.1.1 Introduction to SLE

We can understan how SLE is linked to statistical mechanics if we consider the following example.

Consider the Ising model in a simply connected region D with boundary ∂D, with a very fine lattice inside (essentially, we want the lattice spacing to be much smaller than the system size and the correlation length at a given temperature).

We impose the following boundary conditions, see figure 5.1. On the upper portion of the boundary ∂D between A and B we force the spins to be up and, on the lower portion, to be down. This forces a domain

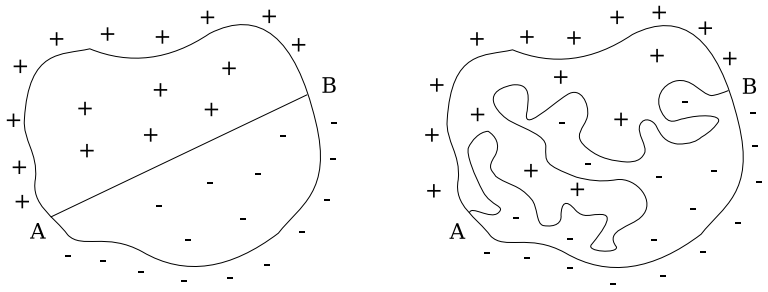

Figure 5.1: The Ising model in a domain D at $T = 0$ (left) and T near T_c (right).

wall to go between the points A and B. Then at zero temperature there will be exactly one straight domain wall between the points A and B. As the temperature increases, the domain wall will wander off the straight line, and eventually, at the critical temperature will become a complicated fractal curve.

The fractal curves that appear at the critical temperature are the ones that the SLE focuses on.

5.1.2 Loewner equation

Consider the upper half-plane $\mathbb{H}$. A compact subset K of $\overline{\mathbb{H}}$, such that $\mathbb{H}\backslash K$ is simply connected and $K = \overline{K \cap \mathbb{H}}$, is called a hull. For any hull K there exists a unique conformal map, denoted by g_K which sends $\mathbb{H}\backslash K$ onto $\mathbb{H}$ and satisfies the normalization

$$\lim_{z\to\infty}(g(z) - z) = 0.$$

This map has an expansion for $z \to \infty$ of the form

$$g(z) = z + \frac{b_1}{z} + \cdots + \frac{b_n}{z^n} + \ldots$$

where all expansion coefficients are real. The coefficient $b_1 = b_1(K)$ is called the capacity of the hull K.

Suppose that $\gamma(t)$ (where $t \geq 0$) is a continuous path in $\overline{\mathbb{H}}$ which starts from $\gamma(0) \in \mathbb{R}$. We allow the path to hit itself or the real line, but if it does, we require the path to reflect off into open space immediately. In other words, the path is not allowed to enter a region which has been

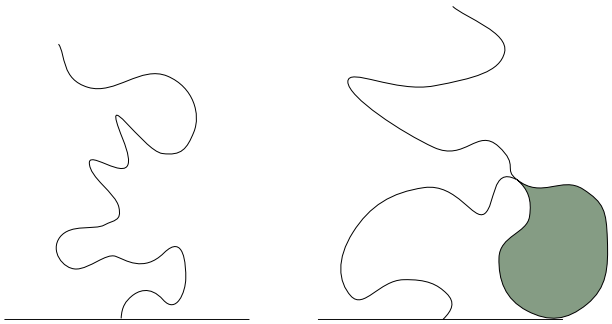

Figure 5.2: Left: a path that doesn't hit itself, the hull is the path. Right: a path that hits itself and the real line, the hull is the path and the gray zone.

disconnected from infinity by $\gamma[0,t] \cup \mathbb{R}$. To be specific, let us denote by H_t for $t \geq 0$ the unbounded connected component of $\mathbb{H}\backslash\gamma[0,t]$, and let K_t be the closure of $\mathbb{H}\backslash H_t$. Then we require that for all $0 \leq s < t$, K_s is a proper subset of K_t. K_t is the hull and $\tau_t = \gamma(t)$ the tip of the curve $\gamma[0,t]$. We see in figure 5.2 two paths satisfying these conditions with their hull.

Given a path $\gamma(t)$ we define $g_t(z) := g_{K_t}(z)$. The function $g_t(z)$ maps the whole boundary of K_t onto part of the real axis. In particular, it maps the tip τ_t to a real point a_t. As the path grows, the point a_t moves on the real axis. It can be proved that a_t is a continuous function in t.

A simple but instructive example is when γ is a straight line growing vertically upwards from a fixed point a: $\gamma(t) = a + i2\sqrt{t}$. In this case, as showed in the previous chapter by equation (4.1),

$$g_t(z) = a + \sqrt{(z-a)^2 + 4t} \tag{5.1}$$

and $a_t = a$.

It can be shown that, given a curve γ, the map g_t satisfies a very simple differential equation called Loewner equation

$$\partial_t\, g_t(z) = \frac{2}{g_t(z) - a_t}\,, \qquad\qquad g_0(z) = z\,. \tag{5.2}$$

We can give an intuitive derivation of this equation. Suppose that we already know the map g_t and want to find out what happens during the time increment between t and $t + \mathrm{d}t$. Using the composition of maps we write $g_{t+\mathrm{d}t} = \mathrm{d}g_t \circ g_t$. Under the map g_t the segment $\gamma[t, t+\mathrm{d}t]$ is

mapped to a (almost) straight short vertical segment beginning at point $a_t \in \mathbb{R}$. By equation (5.1) the conformal map $\mathrm{d}g_t$ removing the segment is

$$\mathrm{d}g_t(z) = a_t + \sqrt{(z-a_t)^2 + 4\mathrm{d}t} \tag{5.3}$$

Composing this with g_t and expanding in small $\mathrm{d}t$ we get

$$\begin{aligned} g_{t+\mathrm{d}t}(z) = \mathrm{d}g_t(g_t(z)) &= a_t + \sqrt{(g_t(z)-a_t)^2 + 4\mathrm{d}t} \approx & (5.4)\\ &\approx g_t(z) + \frac{2\mathrm{d}t}{g_t(z)-a_t}. & (5.5) \end{aligned}$$

This immediately leads to Loewner equation (5.2) in the limit $\mathrm{d}t \to 0$.

There are two ways in which one can think about Loewner equation. The first one was just presented: given a curve γ the upper half-plane, we can obtain, at least in principle, the real function a_t by constructing the corresponding conformal maps. The second way is the opposite: given a real continuous "driving" function a_t we can plug it into Loewner equation and solve it forward in time starting with the initial condition $g_0(z) = z$.

An example: we can consider the driving function $a_t = a$; we can easily solve the Loewner equation (5.2) and we obtain the expected result of equation (5.1).

We explain now how we can find the hull corresponding to a map $g_t(z)$ that solves Loewner equation (5.2) with a driving function a_t. For a given point $z \in \mathbb{H}$, the solution of equation (5.2) is well defined as long as $g_t(z) - a_t \neq 0$. Thus, we define $\bar{t}_z$ as the first time $\bar{t}$ such that $\lim_{t\to\bar{t}}(g_t(z) - a_t) = 0$. For some points z in $\mathbb{H}$ the time $\bar{t}_z = \infty$, meaning that at these points the Loewner map is defined for all times. The union of all the points z for which $\bar{t}_z \leq t$ is the hull corresponding to the map $g_t(z)$:

$$K_t = \left\{ z \in \overline{\mathbb{H}} : \bar{t}_z \leq t \right\}$$

and its complement $H_t = \{z \in \mathbb{H} : \bar{t}_z > t\} = H \backslash K_t$ is the domain of g_t, that is the set of points for which $g_t(z)$ is still defined.

Another useful notion is that of the trace γ produced by Loewner equation. This is defined as the union points

$$\gamma(t) = \lim_{z\to 0} g_t^{-1}(z + a_t)$$

where the limit is taken within the upper half-plane.

Some example. If we consider the driving function $a_t = a$ we find that the hull is equal to the trace.

It's possible to show that the map:

$$g_t(z) = \frac{(z-r)^2 + 2z\sqrt{r^2-2t} + (z+r)\sqrt{(z+r)^2 - 4z\sqrt{r^2-2t}}}{2z} \tag{5.6}$$

is the solution of the Loewner equation with driving function $a_t = 3\sqrt{r^2-2t} - 2r$; for $t < r^2/2$, $g_t(z)$ removes a circular arc of radius r growing in the complex plane from the point r on the real axis towards the point $-r$. The branches of the square roots in equation (5.6) have to be chosen in such a way that

$$\lim_{t \to r^2/2} g_t(z) = \begin{cases} z + r^2/z & \text{for } |z| \geq r, \\ -2r & \text{for } |z| < r. \end{cases} \tag{5.7}$$

Note that at time $\tau = r^2/2$ the map g_t changes discontinuously. At any time before that the hull of the map is the segment of the arc. But exactly at $t = \tau$ the whole region $D = \{|z| < r, \mathrm{Im}\, z \geq 0\}$ (the upper half of the disc of radius r) is mapped to the point $-2r$; then at $t = \tau$ the hull is the region D.

Since now we have discussed the Loewner equation in a deterministic way; in the following we will introduce the Stochastic Loewner Evolution.

5.1.3 Stochastic Loewner Evolution

The remarkable discovery of Schramm [21] was that one can study Loewner equation (5.2) with random driving functions and in this way obtain all possible ensembles of curves with conformally invariant measures. We will not prove, but this it's true if we take $a_t = \sqrt{\kappa} B_t$ where $\kappa > 0$, and B_t is the standard Brownian motion started at $a(0) = 0$. The resulting stochastic Loewner equation is

$$\partial_t\, g_t(z) = \frac{2}{g_t(z) - \sqrt{\kappa} B_t}\,, \qquad\qquad g_0(z) = z\,, \tag{5.8}$$

and the sequence of conformal maps that it produces came to be known as SLE_κ.

We then summarize the properties of SLE_κ:

- for all values of κ one can still define the trace of an SLE_κ as the union of points $\gamma(t) = \lim_{z \to 0} g_t^{-1}(z + a_t)$ (and this limit exists). Moreover,

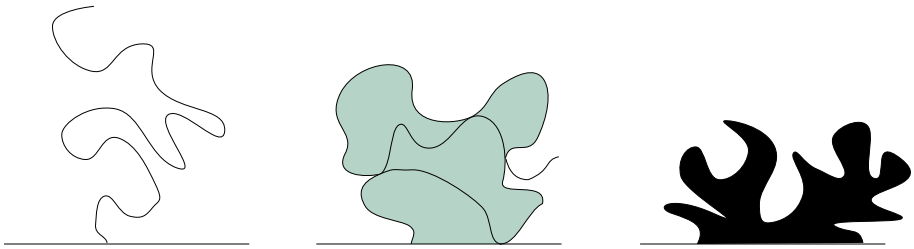

Figure 5.3: Simplified impression of SLE for $\kappa \leq 4$, $4 < \kappa < 8$ and $\kappa \geq 8$ from left to right. The trace of the SLE process is shown in black. The union of the black path and the gray areas represents the hull.

the trace is a continuous curve staring at $\gamma(0) = 0$, reaching infinity as $t \to \infty$ and never crossing itself (self-avoiding).

- For $0 \leq \kappa \leq 4$ an SLE trace γ is a simple curve (does not have double points). In this case the SLE hull coincides with the trace: $K_t = \gamma[0, t]$.

- For $4 < \kappa < 8$ an SLE trace has an infinite number of double points. The trace "touches" both itself and the real axis at every scale.

- For $\kappa \geq 8$ the trace is a space-filling curve: all the points in $\overline{\mathbb{H}}$ lie on the trace.

- The fractal dimension of the trace is

$$d_f(\kappa) = \begin{cases} 1 + \frac{\kappa}{8} & \text{for } \kappa \leq 8, \\ 2 & \text{for } \kappa \geq 8. \end{cases} \tag{5.9}$$

SLE had been introduced by Schramm in [21] in order to prove that LERW (introduced in previous section) is conformally invariant; to do that he proved that the scaling limit of LERW in a domain D converges to the measure of a SLE_2 conformally mapped into the domain D.

Starting from this result, great attention has been posed on SLE, trying to establish connections between SLE and discrete models. The connection is made by defining a path in these discrete models, which in the scaling limit converges to the trace of a SLE process.

Before trying to establish a connection between GPM and SLE, we describe the connection between percolation model and SLE.

5.1.4 SLE and critical percolation

We define site percolation on the triangular lattice as follows. All vertices of the lattice are independently coloured blue with probability p or yellow with probability $1 - p$. An equivalent, and perhaps more convenient, viewpoint is to say that we colour all hexagons of the dual lattice blue or yellow with probabilities p and $1 - p$, respectively. It is well-known that for $p \leq 1/2$, there is almost surely no infinite cluster of connected blue hexagons, while for $p > 1/2$ there exists a.s. a unique infinite blue cluster. This makes $p = 1/2$ the critical point for site percolation on the triangular lattice. For the remainder of this subsection we assume that we are at this critical point.

Let us for now restrict ourselves to the half-plane. Suppose that as our boundary conditions, we colour all hexagons intersecting the negative real line yellow, and all hexagons intersecting the positive real line blue. All other hexagons in the half-plane are independently coloured blue or yellow with equal probabilities. Then there exists a unique path over the edges of the hexagons, starting from the origin, which separates the cluster of blue hexagons attached to the positive real half-line from the cluster of yellow hexagons attached to the negative real half-line. This path is called the chordal exploration process from 0 to ∞ in the half-plane. See figure 5.4 for an illustration.

The exploration process can also be described as the unique path from the origin such that at each step there is a blue hexagon on the right, and a yellow hexagon on the left. This path can also be generated dynamically, as follows. Initially, only the hexagons on the boundary receive a colour. Then after each step, the exploration process meets a hexagon. If this hexagon has not yet been coloured, we have to choose whether to make it blue or yellow, and the exploration process can turn left or right with equal probabilities. But if the hexagon has already been coloured blue or yellow, the exploration path is forced to turn left or right, respectively.

Note that in this dynamic formulation it is clear that the trajectory of the exploration process is determined completely by the colours of the hexagons in the direct vicinity of the path. Further, it is clear that the tip of the process can not become trapped, because it is forced to reflect off into the open if it meets an already coloured hexagon. This suggests that in the continuum limit, when we send the size of the hexagons to zero, the exploration process may be described by a Loewner evolution. The only candidate is SLE_6 , because it can be proved that only SLE_6 has the locality property.

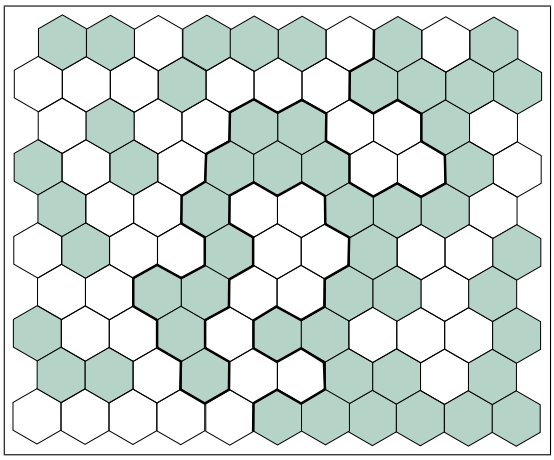

Figure 5.4: Part of the percolation exploration process in the half-plane.

5.2 Paths in critical GPM compared to SLE

In this section we will show how the GPM at the critical point $\rho = 1$ generates naturally non intersecting paths with end points on the boundary (defining properies of a SLE); then we will compare this paths with the SLE and we find that they can correspond to a SLE_4.

5.2.1 Paths in critical GPM

Consider the set $\mathcal{G}$ of $N = L^2$ grid points and an instance $\mathcal{P}$ of $N - 1$ Poisson points. Let $g_1 \in \mathcal{G}$ ($g_2 \in \mathcal{G}$) and define π_1 (π_2) the optimal marriage between $\mathcal{G}_1 := \mathcal{G} \backslash \{g_1\}$ ($\mathcal{G}_2 := \mathcal{G} \backslash \{g_2\}$) and $\mathcal{P}$. We show that the graph $\mathcal{L}$, whose edge set is $\pi_1 \triangle \pi_2 := (\pi_1 \cup \pi_2) \backslash (\pi_1 \cap \pi_2)$ and whose vertex set is the subset of $\mathcal{G} \cup \mathcal{P}$ composed by vertices adjacent to edges in $\pi_1 \triangle \pi_2$, is a path joining g_1 to g_2.

To do this we introduce a point $\bar{p}$ (we can imagine this out of the square) and we define $\hat{\mathcal{P}} := \mathcal{P} \cup \{\bar{p}\}$. We will call $\hat{\pi}_1$ ($\hat{\pi}_2$) the optimal marriage between $\hat{\mathcal{P}}$ and $\mathcal{G}$ such that $\hat{\pi}_1(g_1) = \bar{p}$ ($\hat{\pi}_2(g_2) = \bar{p}$). The set $\hat{\pi}_1 \triangle \hat{\pi}_2$ is composed by edges between the grid and Poisson points that have changed "partner" in $\hat{\pi}_1$ and $\hat{\pi}_2$. We consider the graph $\hat{\mathcal{L}}$ whose edge set is $\hat{\pi}_1 \triangle \hat{\pi}_2$ and whose vertex set is the subset of $\mathcal{G} \cup \hat{\mathcal{P}}$ composed by vertices adjacent to edges in $\hat{\pi}_1 \triangle \hat{\pi}_2$. All the vertices in $\hat{\mathcal{L}}$ have coordination 2; then $\hat{\mathcal{L}}$ is composed by loops. If the instance of Poisson points is not degenerate, we can infer, for geometrical reasons, that $\hat{\mathcal{L}}$ is composed by a single loop containing $\bar{p}$. If we remove from $\hat{\mathcal{L}}$ the vertex $\bar{p}$ and the

edges $(\bar{p}, g_1)$ and $(\bar{p}, g_2)$ we obtain a path joining g_1 to g_2; obviously this graph is equal to $\mathcal{L}$.

Since every Poisson point $p \in V(\mathcal{L})$ has coordination 2, we can replace it and his incident edges (p, g_a) and (p, g_b) with an edge (g_a, g_b). Then we obtain a path on the grid points joining g_1 to g_2.

If we impose L to be odd and we chose g_1 to be the grid point in the middle of the upper boundary of the square and g_2 the grid point in the middle of the lower boundary of the square, we obtain paths like the one shown in figure 5.5.

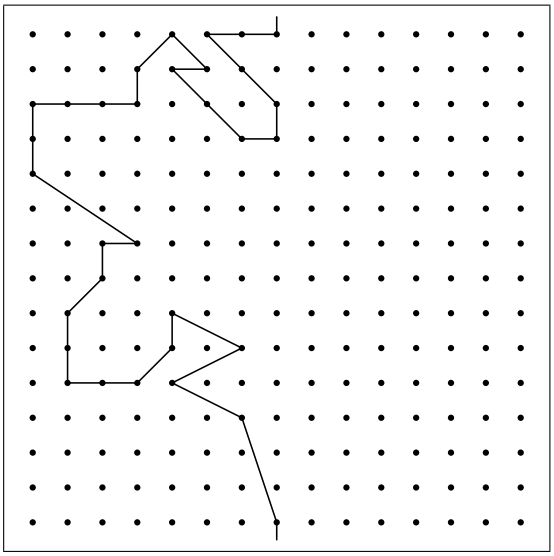

Figure 5.5: A path connecting the grid point in the middle of the upper boundary of the square and the grid point in the middle of the lower boundary of the square, in a square of side $L = 15$.

5.2.2 Paths in critical GPM compared to SLE

We have compared the paths generated by GPM at the critical point with the SLE finding the left passage probability of the points of the square. Consider the square with a fine grid inside; the left passage probability of a point p of this fine grid is the probability that a path generated by the GPM passes at the left of p.

For the SLE_κ it is known the left passage probability for the points of the upper half-plane $\mathbb{H}$. Let us fix a point $z = x + iy \in \mathbb{H}$, then the

probability that a trace of a SLE_κ passes to the left of this point is (Schramm formula)

$$\mathbf{P}\left[\gamma \text{ left of } z\right] = \frac{1}{2} + \frac{\Gamma\left(\frac{4}{\kappa}\right)}{\sqrt{\pi\Gamma\left(\frac{4}{\kappa}-\frac{1}{2}\right)}}\frac{x}{y}\,{}_2F_1\left(\frac{1}{2},\frac{4}{\kappa};\frac{3}{2};-\frac{x^2}{y^2}\right) \tag{5.10}$$

where ${}_2F_1$ is a hypergeometric function [31].

We have mapped this distribution into the square and then we have compared it, for different values of κ, with the left passage probability for the points of the square obtained by simulations with the GPM, performing a sampling of 50.000 paths on a square of side $L = 15$; we compared the contour lines of these two distributions; we see in figure 5.6 that our distribution is very similar to the distribution of a SLE_4.

After that we have found the distribution of the lengths of curves generated with the GPM on a square of side $L = 9, 15, 25$, obtained by a sampling as before, as we see in figure 5.7. The distributions for $L = 9$ and $L = 15$ have been rescaled by a factor c^2 and c rispectively and we obtained that, for a value of $c = 1.165 \pm 0.010$, they are placed one upon another, as we can see in figure 5.8. From this we can then find the fractal dimension d of our curves, given by the relation:

$$d - 1 = \frac{\log c}{\log 5/3} \tag{5.11}$$

since the ratio between following sizes is $5/3$. By equation (5.9), this is the same fractal dimension of a SLE_κ with the following κ:

$$\kappa = 8(d-1) = 2.4 \pm 0.2. \tag{5.12}$$

This result is not consistent with the one obtained from the left passage probability.

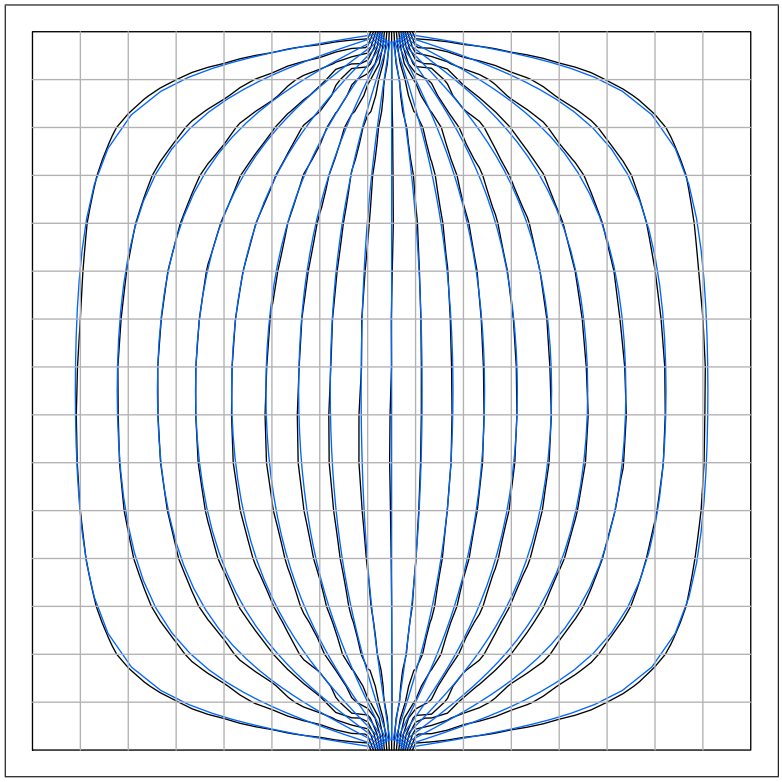

Figure 5.6: Contour lines of the distribution of the left passage probability obtained with the GPM from a sampling of 50.000 paths on a square of side $L = 15$ (in black) and the one of an SLE_4 (in blue).

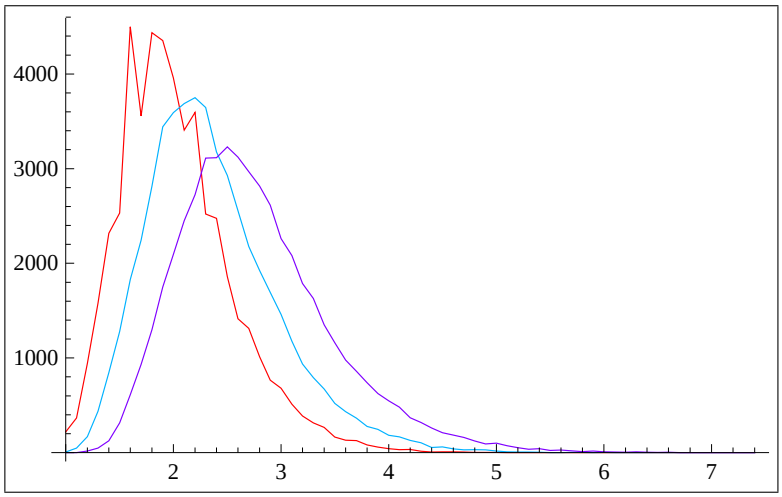

Figure 5.7: The length probability distribution for the curves generated by GPM on a square of side $L = 9$ (red), $L = 15$ (blue) and $L = 25$ (purple) with a sampling of 50.000 paths.

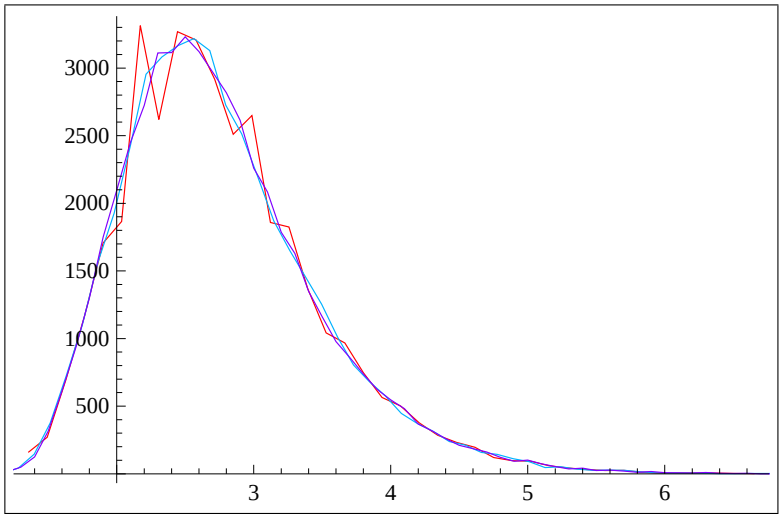

Figure 5.8: The lenght probability distribution of figure 5.7 rescaled of c^2 for $L = 9$ and c for $L = 15$, with $c = 1.165$.

Riassunto in italiano

Capitolo 1

Nel primo capitolo, dopo aver fornito le fondamentali definizioni di teoria dei grafi e una concisa introduzione all'ottimizzazione combinatorica, viene presentato il Grid-Poisson Marriage, il modello di meccanica statistica oggetto di studio del presente lavoro di tesi. Vengono quindi messi in luce i legami esistenti fra tale modello e il noto problema di ottimizzazione combinatorica conosciuto con il nome di Assignment Problem. Viene quindi fornita una descrizione dell'algoritmo ungherese che trova la soluzione di tale problema in tempo polinomiale.

L'ottimizzazione combinatorica è una branca della computer science il cui scopo è trovare la soluzione di problemi il cui insieme di possibli soluzioni ha cardinalità finita. Si consideri il seguente esempio: sono date N macchine e N lavori da compiere, sia ϵ_{ij} il costo necessario alla macchina i per svolgere il lavoro j. Si vuole assegare un lavoro ad ogni macchina minimizzando il costo totale. Quello ore descritto è l'Assignment Problem.

Gli elementi di un problema di ottimizzazione combinatorica sono: una instance del problema, un insieme di possibili soluzioni e una funzione da minimizzare definita sull'insieme delle possibili soluzioni. Per il suddetto problema tali elementi sono rispettivamente: una matrice di costi ϵ_{ij}, l'insieme delle possibili assegnazioni e il costo di ogni assegnazione. Si è interessati a trovare la soluzione dei problemi di ottimizzazione per via algoritmica; si dice che un algoritmo risolve un problema se il tempo impiegato dall'algoritmo per trovare la soluzione del problema è maggiorato da un polinomio nella taglia del problema (un polinomio in N per l'Assignment Problem).

L'algoritmo ungherese (attributo assegnatogli in onore di alcuni matematici ungheresi per i contributi apportati allo sviluppo del medesimo) risolve l'Assignment Problem in un tempo $\mathcal{O}(N^3)$.

Il Grid-Poisson Marriage (GPM) è così definito: consideriamo il quadrato $[0, L] \times [0, L] \subset \mathbb{R}^2$ nel piano, L intero, con metrica euclidea. Definiamo i punti che chiameremo di griglia:

$$\mathcal{G} = \{(i - 0.5, j - 0.5) \in [0, L] \times [0, L] : i \in (1, 2, \ldots, L), j \in (1, 2, \ldots, L)\}$$

(sia $N := |\mathcal{G}| = L^2$) e quelli che chiameremo di Poisson:

$$\mathcal{P} = \{(x_i, y_i) \in [0, L] \times [0, L] : i \in (1, 2, \ldots, M)\}$$

con x_i e y_i variabili aleatorie indipendenti con distribuzione uniforme in $[0, L]$ (sia $M := |\mathcal{P}| \geq N$).

Data una instance di punti di Poisson, definiamo un marriage come una funzione $\pi : \mathcal{G} \to \mathcal{P}$ che assegna ad ogni punto di griglia un punto di Poisson, in maniera tale che nessun punto di Poisson venga assegnato a più di un punto di griglia.

Definiamo l'energia di un marriage π come la somma delle distanze fra punti accoppiati:

$$H_{\mathcal{P}}(\pi) = \sum_{i}^{N} d(i, \pi(i)).$$

Chiameremo π_{opt} il marriage che minimizza l'energia e definiamo come energia di una instance di punti di Poisson l'energia di π_{opt}:

$$H(\mathcal{P}) := H_{\mathcal{P}}(\pi_{opt}) = \min_{\pi} H_{\mathcal{P}}(\pi).$$

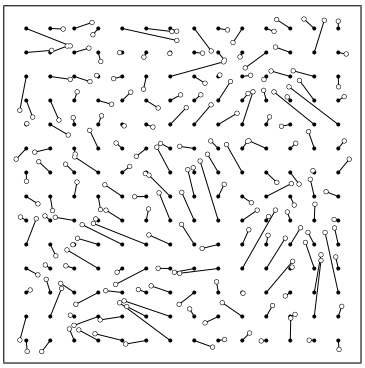

Figure 5.9: π_{opt} per 196 punti di griglia e 196 punti di Poisson.

Vediamo che per trovare l'energia di una instance di punti di Poisson dobbiamo risolvere una variante dell'Assignment Problem in cui la matrice dei costi ϵ_{ij} è sottoposta a vincoli geometrici.

Poiché i punti di Poisson sono estratti con distirbuzione uniforme nel quadrato, è possibile definire $\langle H(\mathcal{P})\rangle_{\mathcal{P}}$ come la media di $H(\mathcal{P})$ rispetto a tale distribuzione.

Capitolo 2

In questo capitolo studieremo il comportamento di $\langle H(\mathcal{P})\rangle_{\mathcal{P}}$ in funzione della taglia N del sistema e di un parametro densità definito come $\rho := M/N$; scopriremo un comportamento particolare per $\rho = 1$. Faremo questo conducendo simulazioni numeriche e introducendo due euristiche: lo Stable Marriage algorithm e il Box Algorithm.

Un'euristica è un'algoritmo che non trova la soluzione ottimale di un problema di ottimizzazione combinatorica, ma è ha il vantaggio di essere più veloce o più semplice da trattare analiticamente.

Lo Stable Marriage algorithm è un algoritmo di ottimizzazione locale; consideriamo due insiemi discreti di punti $U, V \subseteq \mathbb{R}^d$; diremo che due punti $x \in U$ e $y \in V$ sono "mutually closest" se y è il punto più vicino a x in V e x è il punto più vicino a y in U. Data una configurazione di punti, uniamo tutte le coppie di punti che sono "mutually closest" e le rimuoviamo; ripetiamo indefinitamente. Se applichiamo questo algoritmo al GPM, chiameremo la configurazione otteneuta π_{st}; è quindi vera la seguente disuguaglianza:

$$H_{\mathcal{P}}(\pi_{opt}) \leq H_{\mathcal{P}}(\pi_{st}) \, .$$

Abbiamo implementato lo Stable Marriage algorithm che trova la soluzione in tempi polinomiali $\mathcal{O}(N^2)$.

Il Box algorithm è un algoritmo del tipo "divide and conquer". Consiste nel dividere il quadrato di lato L del GMP in quadrati di lato 1 e unire tutte le possibili coppie di punti di griglia e di Poisson presenti nel quadrato di lato 1 e rimuoverle; si uniscono le coppie di quadrati adiacenti a formare un rettangolo e si uniscono tutte le possibili coppie di punti di griglia e di Poisson presenti nel rettangolo e si rimuovono; si ripete il secondo step ora descritto fino a che tutti i punti sono stati accoppiati. Chiameremo la configurazione otteneuta π_{box}; è quindi vera la seguente disuguaglianza:

$$H_{\mathcal{P}}(\pi_{opt}) \leq H_{\mathcal{P}}(\pi_{st}) \leq H_{\mathcal{P}}(\pi_{box}) \, .$$

É stata trovata una stima per eccesso di $\langle H_{\mathcal{P}}(\pi_{box})\rangle_{\mathcal{P}}$ e quindi di $\langle H_{\mathcal{P}}(\pi_{opt})\rangle_{\mathcal{P}}$, per un sistema con N punti di griglia; si evidenziano comportamenti differenti in funzione della densità ρ:

$$\langle H_{\mathcal{P}}(\pi_{opt}, N)\rangle_{\mathcal{P}} \lesssim \langle H_{\mathcal{P}}(\pi_{st}, N)\rangle_{\mathcal{P}} \lesssim \begin{cases} N & \text{if } \rho \neq 1 \\ N \ln N & \text{if } \rho = 1 \end{cases} \quad N \to \infty \,. \tag{5.13}$$

Sono quindi state fatte simulazioni numeriche con lo Stable Marriage algorithm e con l'Hungarian algorithm per valutare gli andamenti di $\langle H_{\mathcal{P}}(\pi_{st}, N)\rangle_{\mathcal{P}}$ e di $\langle H_{\mathcal{P}}(\pi_{opt}, N)\rangle_{\mathcal{P}}$ al crescere di N, al variare di ρ. I risultati sono riportati in figura 5.10. Sono stati visti i due regimi, in accordo con la (5.13), e si può affermare che per $\rho = 1$ l'energia è una quantità superestensiva. Questo comportamento particolare in $\rho = 1$, messo in luce dalle simulazioni, fa pensare ad una cirticità del GPM per tale valore.

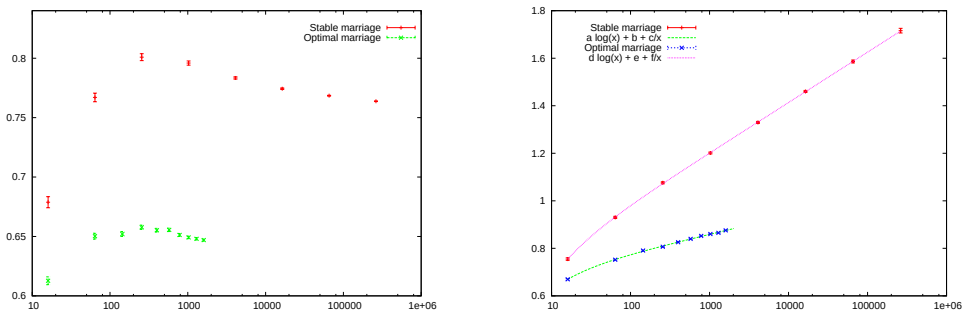

Figure 5.10: Sinistra: plot di $\frac{\langle H_{\mathcal{P}}(N)\rangle_{\mathcal{P}}}{N}$ vs N per $\rho = 17/16$. Destra: plot di $\frac{\langle H_{\mathcal{P}}(N)\rangle_{\mathcal{P}}}{N}$ vs N per $\rho = 1$.

Capitolo 3

Abbiamo ipotizzato criticità per il GMP a $\rho = 1$; lo studio dei fenomeni critici è una delle sfide della meccanica statistica; il comportamento di un sistema al punto critico è caratterizzato dal divergere della lunghezza di correlazione e non può essere facilmente approssimato da un sistema di piccola taglia. Il Finite Size Scaling (FSS) è un ottimo metodo per estrapolare risultati nel limite termodinamico ottenuti da simulazioni (o esperimenti) su sistemi finiti.

In questo capitolo viene prima data una concisa trattazione del FSS, viene quindi definita una funzione di correlazione per il GPM; viene ricavata la lunghezza di correlazione da simulazioni numeriche e si verifica se

questa rispetta le predizioni del FSS.

Consideriamo un sistema di taglia L controllato da un parametro assimilabile alla temperatura T, sia $t = (T - T_c)/T_c$. Sappiamo che per $t \to 0$ la lunghezza di correlazione ξ_∞ diverga: $\xi_\infty \sim |t|^{-\nu}$; sia $\mathcal{O}_L(t)$ un'osservabile del sistema a taglia L, che si comporti per $|t| \to 0$ come $\mathcal{O}_\infty(t) \sim |t|^{-x_\mathcal{O}}$. Possiamo scirvere $\mathcal{O}_L(t)$ come una funzione di $\xi_\infty(t)$ e L:

$$\mathcal{O}_L(t) \approx f_\mathcal{O}(\xi_\infty(t), L) \, .$$

Non svilupperemo qui la trattazione del FSS, ma ne esporremo solo i risultati; un primo risultato, che prende il nome di Asymptotic FSS, consiste nella relazione:

$$\mathcal{O}_L(t) \approx L^{x_\mathcal{O}/\nu} G_\mathcal{O}(tL^{1/\nu}) \, ; \tag{5.14}$$

un secondo risultato, che prende il nome di Correlation Lenght FSS, consiste nella relazione:

$$\frac{\mathcal{O}_{\alpha L}(t)}{\mathcal{O}_L(t)} \approx F_\mathcal{O}\left(\frac{\xi_L(t)}{L}\right) \, . \tag{5.15}$$

Introduciamo quindi una funzione di correlazione per il GPM; data una instance di punti di Poisson e trovato il marriage ottimale, possiamo associare ad ogni punto di griglia con coordinate $\vec{x}$ un vettore $\vec{\varphi}(\vec{x})$ applicato in $\vec{x}$ che termina nel punto di Poisson accoppiato. Introduciamo nel GPM condizioni al bordo toroidali e definiamo la funzione di correlazione:

$$G_L(\vec{r}) = \sum_{\vec{x}} \langle \frac{\vec{\varphi}(\vec{x}) \cdot \vec{\varphi}(\vec{x}+\vec{r})}{|\vec{\varphi}(\vec{x})||\vec{\varphi}(\vec{x}+\vec{r})|} \rangle_\mathcal{P} \, ,$$

e la funzione di correlazione Wall-to-Wall:

$$G_{W,L}(y) = \sum_x G_L(x,y)$$

Se scegliamo come osservabile $\mathcal{O}_L$ la funzione di correlazione ξ_L, le relazioni (5.14) e (5.15) diventano:

$$\frac{\xi_L(t)}{L} \approx G_\xi(tL^{1/\nu}) \tag{5.16}$$

e (ponendo $\alpha = 2$)

$$\frac{\xi_{2L}(t)}{\xi_L(t)} \approx F_\xi\left(\frac{\xi_L(t)}{L}\right) \, . \tag{5.17}$$

Il nostro metodo di indagine è stato: abbiamo effettuato simulazioni numeriche a differenti taglie L e differenti ρ (nel nostro caso $t = \rho - 1$) e abbiamo estrapolato la lunghezza di correlazione $\xi_L(t)$. Quindi, se è vero che il GPM è critico a $\rho = 1$, deve esistere un valore di ν tale che le coppie di punti $(\xi_L(t)/L, tL^{1/\nu})$ collassano su una curva. Vediamo ad esempio che prendendo $\nu = 5/4$, o valori prossimi a questo, la relazione di scaling (5.16) è verificata, figura 5.11 (sinistra). Per quanto riguarda la relazione di scaling 5.17, abbiamo fatto simulazioni a $L = 20, 22$ e abbiamo estrapolato la lunghezza di correlazione; plottando $\frac{\xi_{2L}(t)}{\xi_L(t)}$ vs $\frac{\xi_L(t)}{L}$, vediamo che i punti cadono con una buona approssimazione su una curva, figura 5.11 (destra).

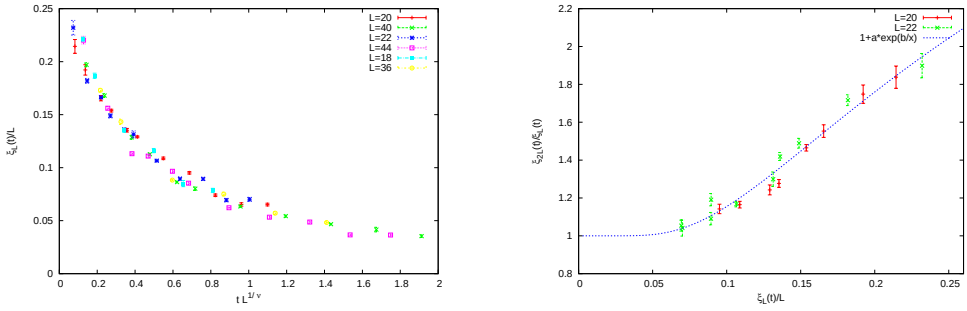

Figure 5.11: Sinistra: Plot di $\xi_L(t)/L$ vs $tL^{1/\nu}$ per $\nu = 5/4$. Destra: plot di $\frac{\xi_{2L}(t)}{\xi_L(t)}$ vs $\frac{\xi_L(t)}{L}$; la curva di fit è $F_\xi(x) = a \exp(-0.3/x)$.

Capitolo 4

In questo capitolo vengono inizialmente presentati i principali risultati riguardo le mappe conformi, come il Riemann mapping theorem e la formula di Schwarz-Christoffel. Viene quinidi mostrato come sia possiblie generare alberi spanning (grafi connessi che non contengano loop) con vertici i punti di griglia del GMP sfruttando l'algoritmo ungherese. Si è quindi interessati a testare se tali alberi presentano invarianza conforme.

Il test utilizzato per testare l'invarianza conforme degli alberi è stato proposto da D. B. Wilson; consideriamo un albero spanning sui punti di griglia; ci sarà un unico cammino che connette tre punti agli angoli del quadrato, chiameremo punto triplo l'unico punto dove questi cammini si incontrano. Il test utilizzato è il segunte: è stata trovata la distribuzione del punto triplo nel quadrato; questa è stata quindi mappata con una mappa

conforme nel cerchio; se gli alberi presentano invarianza conforme, allora la distribuzione del punto triplo mappata nel cerchio deve essere invariante sotto rotazioni di 120°; se questa non lo è non c'è motivo di credere che gli alberi siano invarianti conformi. Vediamo in figura 5.12 (sinistra) la distribuzione del punto triplo mappata nel cerchio, e (destra) la differenza di tale distribuzione con se stessa ruotata di 120° (rosso significa differenza positiva e blu negativa). Da questi risultati è difficile affermare se ci sia o meno invarianza conforme.

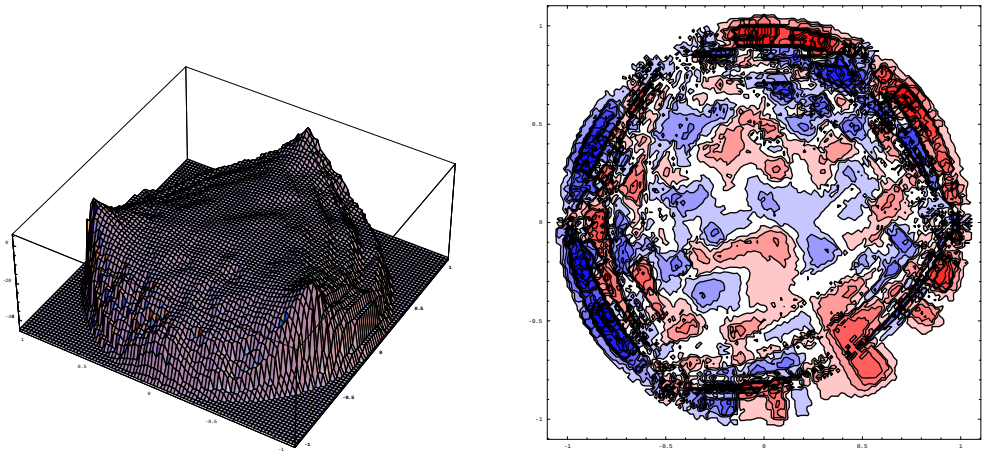

Figure 5.12: Sinistra: distribuzione del punto trioplo mappata nel cerchio. Destra: differenza della precedente distribuzione con se stessa ruotata di 120° (rosso significa differenza positiva e blu negativa.

Capitolo 5

In questo capitolo viene introdotta la teoria conosciuta con il nome si Stochastic Loewner Evolution (SLE); tale teoria permette di descrivere mediante una semplice equazione differenziale stocastica le famiglie di curve del semi-piano complesso che presentano invarianza conforme; tali famiglie dipendono da un unico parametro κ, che interviene nell'equazione differenziale, e possono quindi essere catalogate in base a questo. Vediamo in figura 5.13 alcuni esempi di curve in funzione di κ. Diversi modelli di meccaninca statistica al punto critico generano curve che si suppone godano di invarianza conforme e che quindi possano essere descritte mediante SLE. Anche se questa rimane, allo stato attuale, solo una congettura per molti modelli, dimostrazioni rigorose sono state trovate per il Loop

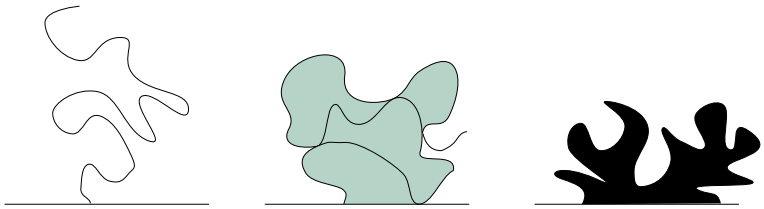

Figure 5.13: Esempi di SLE per diversi valori di κ: sinistra: $\kappa \leq 4$, centro: $4 < \kappa < 8$ e destra: $k \geq 8$.

Erased Random Walk da O. Schramm. Viene quindi dato un dettagliato esempio riguardo come il modello di percolazione al punto critico genera curve che potrebbero essere descritte da una SLE con $\kappa = 6$.

Viene quindi illustrato come anche il GPM al valore critico di $\rho = 1$ genera dei cammini sui punti di griglia. Si è quindi testato se tali cammini possono essere descritti mediante delle SLE. Per fare questo si è trovata (mediante simulazioni) la left passage probability per i punti del qudrato, ovvero la probabilità che un cammino passi a sinistra di un dato punto. Questa è stata quindi confrontata con quella ricavata analiticamente per una SLE; in figura 5.14 vengono messe a confronto le linee di livello di tale probabilità per il GPM e per una SLE con $\kappa = 4$. Sembra esserci un discreto accordo.

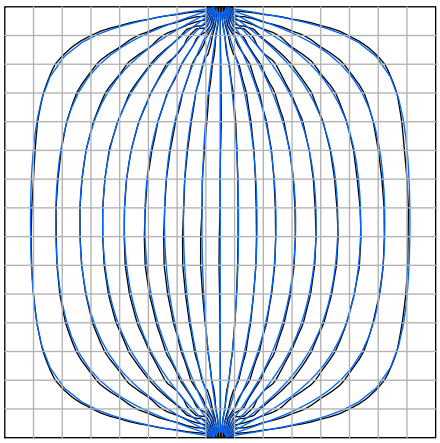

Figure 5.14: Confronto fra le linee di livello della left passage probability per il GPM (nero) e per una SLE con $\kappa = 4$ (blu).

Bibliography

[1] M. Mézard, G. Parisi, M. A. Virasoro, *Spin Glass Theory and Beyond*, Word Scientific, Singapore, 1987.

[2] A. Holroyd, R. Pemantle, Y. Peres, O. Schramm, *Poisson Matching*, arXiv:0712.1867v (2007).

[3] C. Hoffman, A. Holroyd, Y. Peres *A stable marriage of Poisson and Lebesgue*, Annals of Probability 2006, Vol. 34, No. 4, 1241-1272;arXiv:math/0505668v4 [math.PR].

[4] M. R. Garey, D. S. Johnson, *Computers and Intractability: A Guide to the Theory of NP-Completeness*, New York, W.H. Freeman and Company, 1979.

[5] O. Kallenberg, *Random measures*, Akademie-Verlag, Academic Press, 1976.

[6] G. Monge, *Mémoire sur la théorie des déblais et des remblais*, Histoire de l'Académie Royale des Sciences [année 1781. Avec les Mémoires de Mathématique & de Physique, pour la même Année] (2e partie) (1784) [Histoire: 34-38, Mémoire:] 666-704.

[7] A. Schrijver, *On the history of combinatorial optimization* (till 1960), "Handbook of Discrete Optimization" (K. Aardal, G.L. Nemhauser, R. Weismantel, eds.), Elsevier, Amsterdam, 2005, pp. 1–68.

[8] H. Kuhn, *The Hungarian Method for the assignment problem*, Naval Research Logistics Quarterly, 2:83-97, 1955.

[9] L. Lovász, M. D. Plummer, *Matching theory*, North-Holland, 1986.

[10] D. E. Knuth, *The Stanford GraphBase: A Platform for the Combinatorial computing*, Addison-Wesley, (1993).

[11] M. Mèzard and G. Parisi, *Replicas and optimization*, J. Physique Lett. 46, L771 (1985).

[12] G. Parisi, *A Conjecture on random bipartite matching*, arXiv:cond-mat/9801176.

[13] D. J. Aldous, *The $\zeta(2)$ limit in the random assignment problem*, Random Struct. Algorithms, v.18 n.4, p.381-418, 2001.

[14] C.Nair, B. Prabhakar, M. Sharma, *Proofs of the Parisi and Coppersmith-Sorekin random assignement conjecture*, Random Struct. Algorithms, Vol. 27, Num. 4, 2005.

[15] D Gale and L. Shapley, *College admissions and stability of marriage*, Amer. Math. Monthly, 69(1):9-15, 1962.

[16] M. X. Goemans and D. P. Williamson, *The Primal-Dual Method for Approximation Algorithms and its Application to Network Design Problems*, in Approximation Algorithms, D. Hochbaum, Ed., 1997.

[17] P. Embrechts, C. Kluppelberg, T. Mikosch, *Modelling Extremal Events for Insurance and Finance*, Springer Verlag, 1997.

[18] M. N. Barber, *Finite Size Scaling*, in Phase Transitions and Critical Phenomena, edited by C. Domb and J. L. Lebowitz, Vol. 8 (Academic Press, London, 1983).

[19] S. Caracciolo, R. G. Edwards, S. J. Ferreira, A. Pelissetto and A. D. Sokal, *Extrapolating Monte Carlo Simulations to Infinite Volume: Finite-Size Scaling at $\xi/L \gg 1$*, Phys. Rev. Lett. 74, 2969 (1995), e-print hep-lat/9409004.

[20] D. Fichera, *Cavity Methods in Optimization Problems: Exact and Approximated Algorithms.*, Ph.D. Thesis, at Università degli Studi di Milano (2007-2008).

[21] O. Schramm, *Scaling limits of loop-erased random walks and uniform spanning trees*, Israel J. Math. 118 (2000), 221-288

[22] G. F. Lawler, O. Schramm, W. Werner, *Conformal invariance of planar loop-erased random walks and uniform spanning trees*, Ann. Probab. 32:1B (2004), 939-995

[23] M. Aizenman, A. Burchard, C. M. Newman, D. B. Wilson, *Scaling Limits for Minimal and Random Spanning Trees in Two Dimensions*, Random Structures and Algorithms, v. 15 (1999), 319–367.

[24] D. B. Wilson, *Generating random spanning trees more quickly than the cover time*, Proceedings of the Twenty-eighth Annual ACM Symposium on the Theory of Computing (Philadelphia, PA, 1996), 296-303, ACM, New York, 1996.

[25] D. B. Wilson, *On the Red-Green-Blue Model*, Phys. Rev. E 69, 037105 (2004).

[26] C. Amoruso, A.K. Hartmann, M.B. Hasting, M.A. Moore, *Conformal Invariance and SLE in Two-Dimensional Ising Spin Glasses*, P.R.L. 97, 267202 (2006).

[27] D. Bernard,P. Le Doussal, A.A. Middleton, *Are Domain Walls in 2D Spin Glasses described by Stochastic Loewner Evolutions?*, P.R.B. 76 020403(R) (2007) (cond-mat/0611433).

[28] J. Cardy, *SLE for theoretical physicists*, Annals Phys. 318 (2005) 81-118.

[29] W. Kager, B. Nienhuis, *A Guide to Stochastic Loewner Evolution and its Applications*, J. Stat. Phys. 115:1149-1229 (2004).

[30] I. A. Gruzberg, *Stochastic geometry of critical curves, Schramm-Loewner evolutions, and conformal field theory*, J.Phys. A39 (2006) 12601-12656.

[31] M. Abramowitz, I. A. Stegun, *Handbook of Mathematical Functions with Formulas, Graphs, and Mathematical Tables*, "Hypergeometric Functions", Ch. 15; New York: Dover, pp. 555-566, 1972.

[32] M. Abramowitz, I. A. Stegun, *Handbook of Mathematical Functions with Formulas, Graphs, and Mathematical Tables*, "Elliptic Integrals." Ch. 17; New York: Dover, pp. 587-607, 1972.